Politecnico di Torino

Politecnico di Torino

Master's Degree in Electronic Engineering
A.A. 2024/2025
Graduating Session: March 2025

ADVANCED LARGE-SIGNAL ELECTROTHERMAL MODEL FOR RF HBT

Supervisors:
Prof. Marco Pirola
Prof.ssa Chiara Ramella

Candidate:
Di Fede Gaetano

Contents

Acknowledgement iii

Abstract. iv

1. Introduction 1

1.1.The Bipolar Junction Transistor. 1

1.1.1. Structure and Operative Mode. 1

1.1.2 The Currents of the Transistor. 3

1.1.3 From the BJT to the HBT. 6

2.Description of the BJT equivalent models 9

2.1.Ebers-Moll Model of a BJT. 9

2.1.1.Static Model 9

2.1.2. Ebers-Moll Large-Signal Model 15

2.1.3.Erbes-Moll Small-Signal 19

2.2.Gummel-Poon Model. 21

2.2.1. Static Model 21

2.2.2 Gummel-Poon Large-Signal and Small-Signal Model. 31

2.3.1 Temperature dependence of BJT model parameters. 36

3. Customized implementation of the Gummel-Poon Model in ADS 37

3.1. Derivation and implementation of the model 37

3.1.1 DC Model Derivation. 38

3.1.2 DC Model Testing. 41

3.1.3 AC Model Derivation. 44

3.1.4 AC Model Testing. 47

3.1.5 Thermal Model Derivation. 52

3.1.6. Thermal Model Testing. 55

4.Implementation of class A and Class B amplifier 59

4.1. Design of the amplifiers and testing 59

4.1.1. Class A amplifier and testing 59

4.1.2. Class B amplifier and testing 66

5.Conclusions 72
Bibliography 73

Acknowledgement

I would like to express my gratitude to all those who have supported me throughout my academic journey over the years. I am especially grateful to my wife for her unwavering love, patience, and, most importantly, for being the driving force behind my perseverance. I would also like to extend my heartfelt thanks to my parents-in-law for their continuous support and encouragement, as well as to my late parents for their enduring influence. Lastly, I wish to sincerely thank Professor Pirola and PhD student Zhang Wenjun for their invaluable guidance and patience throughout the development of this work.

Abstract.

This paper presents a thermo-electrical model for GaAs Heterojunction Bipolar Transistors (HBTs) at radio frequency, based on the widely used Spice Gummel-Poon model for BJT device simulation. The theoretical framework related to BJT behavior is derived from Massorbio's Book [1]. The objective of this work is to model and simulate the self-heating effect inside GaAs HBTs, which is a critical side effects observed in such devices when operating at high power levels. Specifically, as the dissipated power increases, so does the junction temperature, which consequently leads to a reduction in the collector current.

To demonstrate this phenomenon, the chapter 1 of this thesis provides a comprehensive review of BJT physics and highlights the key differences between homojunction and heterojunction transitions. The chapter 2 details the transition from the Ebers-Moll model to the Gummel-Poon model, with an emphasis on the equations that describe the temperature dependence of the principal parameters. The chapter 3 discusses the model implementation and its validation using Keysight ADS software, where a comparison is made between the Gummel-Poon and Ebers-Moll models, showing excellent agreement between the two.

Finally, the chapter 4 presents three case studies: a tuned Class A amplifier, a tuned Class B amplifier. These examples illustrate that, for the Class A amplifier, the transistor temperature decreases as the input power increases, while for the Class B amplifiers, the temperature increases with input power.

1. Introduction

In this chapter, fundamental aspects regarding the physics, structure, and operating principles of a Bipolar Junction Transistor (BJT) are presented. Subsequently, the Heterojunction Bipolar Transistor (HBT) is examined, with a detailed discussion of its behavior. In particular, the relationship between the HBT and the BJT is explored, highlighting the key differences between the two devices.

1.1.The Bipolar Junction Transistor.

In this paragraph, the principal facts about the physical structure of the BJT and the operative modes will be illustrated; In particular, this will be discussed in 1.1.1 together with some basic facts about the physics behind the inner working of the BJT. In 1.1.2 instead, the expressions for the currents will be illustrated. Lastly in 1.1.3 the HBT is illustrated and how it is connected to the BJT modelling.

1.1.1. Structure and Operative Mode.

A BJT is composed of two PN junctions which are built upon the same substrate forming a NPN or PNP structure; where it is possible to distinguish the two junctions, J_1 and J_2 forming three regions [2], which are illustrated in Fig.1.

Therefore, one can identify the first junction J_1 as the PN junction between collector and base (BC) and the second junction J_2 as the PN junction between base and emitter (BE).

In the external part of the device, there are three metallic terminations to apply voltages or currents and as the Kirckhoff laws imply, only two out of three voltages and currents are actually independent [2].

The device's behavior will depend on the voltages applied to its terminals. In particular, by applying a voltage between the base and emitter pins, denoted as V_{BE}, the behavior of junction J_1 will change, while applying a voltage between the base and collector, denoted as V_{BE}, will modify the behavior of junction J_2, thereby determining the device's overall behavior. [2].

There are four possible ways of biasing a BJT and those are when [2]:

- The BE junction is in the forward biased while the BC junction is in the reverse biased, this state is known as the Forward Active Region or simply Active Region; and this is the region where the BJT works as an amplifier.
- The BE junction is in the reverse biased while the BC junction is in the forward biased, this operative mode is known as the Reverse Active Region or simply the Reverse Region. In this region there is a qualitative behavior that is identical to the Forward Active Region, but it suffers of lower gain; this is due to the fact that in reality the emitter and the collector are never symmetrical.

- Both the base-emitter (BE) junction and the base-collector (BC) junction are forward biased. This operating region is referred to as the saturation region, where the device approximates the behavior of a closed switch.
- Finally, both junctions are reverse biased, a condition known as the cutoff region, where the BJT operates as an open switch.

The last two operating regions, i.e. the saturation and off regions, can be used to implement logic ports.

In the active region, as mentioned, the BE junction is forward biased; this fact implies that a significant current is passing through this junction.

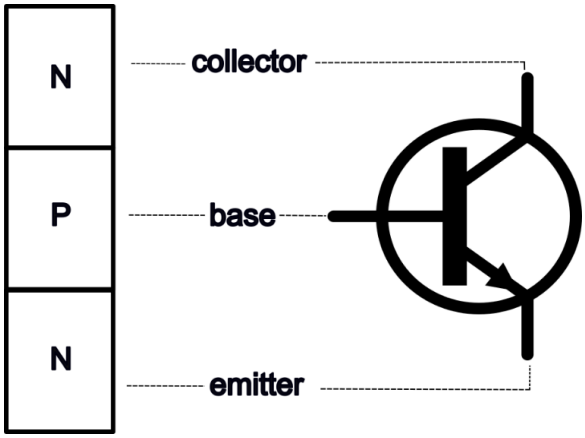

Fig.1 NPN BJT structure and symbol.

Such current, indicated with $-I_E$ in Fig.1, is the summation of two contributions.

Particularly, the electron's injections from the n-type emitter to p-type base is modulated by the voltage V_{BE} in an exponential fashion, as it should be in a forward bias junction. In contrast to what happens in a diode, where a recombination process takes place inside the type-p side according to the following law [2]:

$$n_B(x) = n_B(0)e^{-x/L_{nB}} \qquad (1.1)$$

where $n_B(0)$ is the electron's concentration at the junction and L_{nB} is the base electron's diffusion length base type-p region, see Fig. 2, inside the BJT the base width W_B is much smaller than L_{nB} leading to a minimal electron recombination effect.

As result, the base region is overflown with electrons and these electrons are easily collected by the collector.

In active region, the collector current almost remains constant for a given value of base current; indeed, as it will be shown later, I_C is proportional to the I_B.

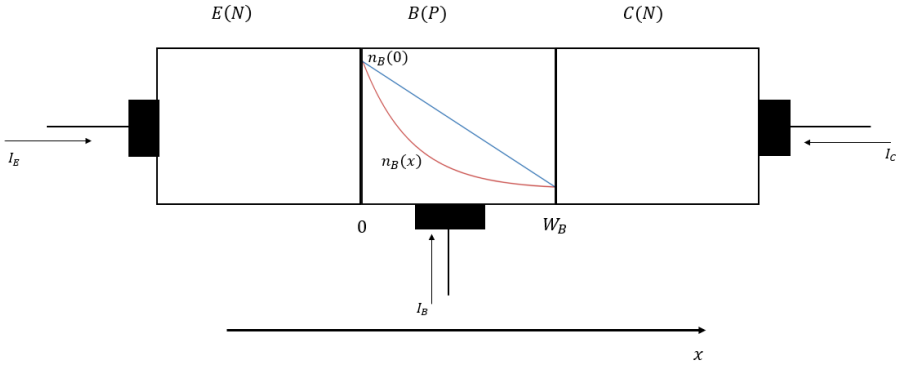

Fig. 2 The electrons concentration behavior inside BJT when working in the active region,

the blue curve indicates the ideal case, whereas

the red curve is closer to the real electrons' concentration behavior.

1.1.2 The Currents of the Transistor.

The emitter current is the current flowing in the base- emitter junction. This current is given by the summation of two contributions due to the flow of two types of carriers, i.e. electrons and holes [2]:

$$I_E = -I_{En} - I_{Ep}$$

the convention for the current's sign is indicated in Fig.3; where it has been assumed that currents and voltages have opposite direction. Whereas for the two components I_{En} and I_{Ep} the real direction of flowing these currents has been chosen as the positive one in the forward active region.

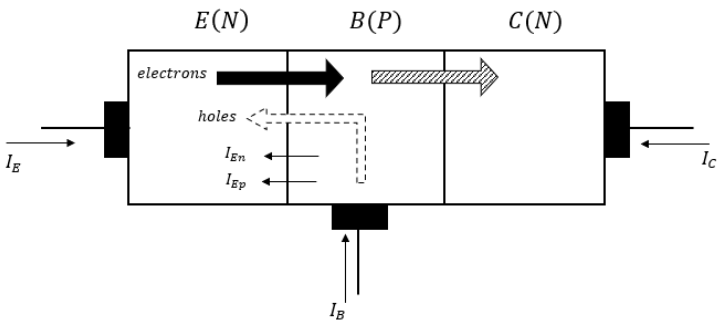

Fig.3 Current Involved for defining the emitter efficiency.

Under forward biased conditions, one has that:

- I_{En} is due to the electrons that are injected by the emitter into the base
- I_{Ep} is due to the holes that are injected by the base into the emitter.

BJTs have a higher doping in the emitter region than the base, i.e. $N_E \gg N_B$ leading to $I_{En} \gg I_{Ep}$; this means that the current I_E is being dominated by the electron from the emitter.

The relation between the two currents I_E and I_{En} can be rewritten by introducing a factor, the emitter efficiency, γ smaller than one [2]:

$$I_{En} = -\gamma I_E$$

where it can be shown that

$$\gamma = \begin{cases} \left[1 + \dfrac{N_B w_B D_{pE}}{N_E x_E D_{nB}}\right]^{-1} & x \ll L_{pE} \\ \left[1 + \dfrac{N_B w_B D_{pE}}{N_E L_{pE} D_{nB}}\right]^{-1} & x \gg L_{pE} \end{cases} \tag{1.2}$$

with x_E being the width of the emitter, L_{pE} the diffusion length, w_B is the base width, N_B and N_E are the density carrier's concentrations in the base and emitter respectively, D_{jE} for $j = n, p$ is the diffusion constant for the electrons/holes in the Emitter, similarly D_{jB} is the diffusion constant for the electrons/holes in the Base .

It should be noted, as illustrated in Fig.3, that the hole trajectory forms a closed path from the emitter pin to the base pin. In contrast, the electrons originating from the base have the potential to flow into the collector, thereby giving rise to the so-called transistor effect. This effect refers to the phenomenon where the collector current is controlled by the base-emitter junction voltage. Consequently, transistor effects can be represented as a controlled current source, as will be demonstrated in the following sections, where the Ebers-Moll model is presented.

Regarding the collector current, it also consists of two contributions, those are:

- the current I_{Cn} resulting from the electrons that traverse the base region and are subsequently gathered by the collector.
- the current I_{C0} which is the inverse saturation current of BC junction.

For this reason, the collector is written as (see Fig.4)

$$I_C = I_{Cn} + I_{C0} \tag{1.3}$$

Since the base length W_B needs to be much smaller than the electrons diffusions length L_{nB}, so that the transport from the emitter to the base of a high percentage of minority carriers is achieved. Moreover, the excess concentration of minority carries, that are injected from the opposite side of the junction, progressively decreases moving through the quasi-neutral region.

This decrease has a different trend depending on the relative size of the width of the quasi-neutral region and the diffusion length. In the case of the BJT, the base region is such that the following condition holds always true [2]:

$$W_B \ll L_{nB}$$

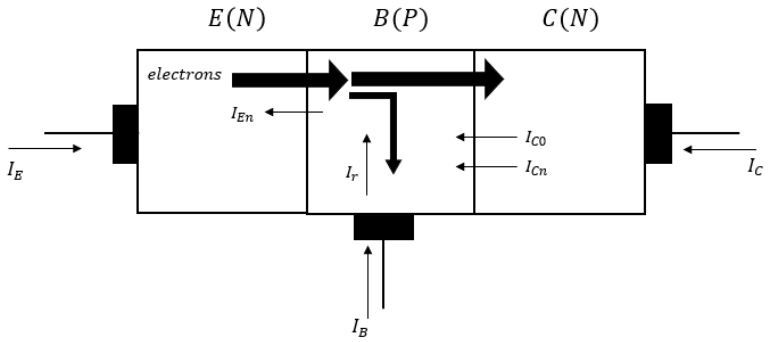

Fig.4 Collector current components.

A linear distribution of the carrier's concentration can be assumed, then this implies the presence of a constant diffusion current associated to the carriers; moreover, it can be shown that such current is inversely proportional to the width of the quasi-neutral region.

Since, the base of the BJT has small width, the current associated with the diffusion of the electrons through the base is significant and in the real devices it is dominant with respect to the inverse saturation current that is present at the BC junction; Therefore, the following approximation for the collector current can be applied

$$I_C \approx I_{Cn}$$

Taking into account that recombination is a static phenomenon involving a quantity of carriers proportional to those injected, it follows that the injected current from the emitter I_{En} and the current delivered to the collector I_{Cn} are proportional to the carrier concentrations at the emitter and collector junctions, respectively. This proportional relationship is characterized by a factor that quantifies the recombination effect occurring in the base, known as the transport factor α_T [2].Taking into account that recombination is a static phenomenon involving a quantity of carriers proportional to those injected. In the active region, the collector current is therefore rewritten as:

$$I_C \approx I_{Cn} = \alpha_T I_{En}$$

the recombination leads to α_T always lesser than 1, even if its value can be very close to the unity [2].

At this point, it is easy to obtain the base current by means of the usual relationship between the three current of the BJT, in fact referring to the current's direction indicated in Fig.1, the base current can be written as [2]:

$$I_B = -I_E - I_C$$

therefore, since I_C and I_E can be rewritten as

$$I_C = I_{Cn} + I_{C0}$$

$$I_E = -I_{En} - I_{Ep}$$

one obtains

$$I_B = I_{En} + I_{Ep} - I_{Cn} - I_{C0}$$

and, since the recombination current is defined as

$$I_r = I_{En} - I_{Cn}$$

the final result for the base current is

$$I_B = I_{Ep} + I_r - I_{C0}$$

Lastly, it should be noted that the I_{C0} current is always negligible [2]. Under ambient temperature conditions, the currents I_{Ep} and I_r are also typically negligible in high-quality BJTs.

Consequently, considering these factors, the following results can be derived:

$$I_C \approx \alpha_T I_{En}$$
$$I_{En} \approx -\gamma I_E$$

from which one defines the forward gain current α_F as:

$$\alpha_F = \frac{I_{En}}{I_E} = \gamma \alpha_T \tag{1.4}$$

then:

$$I_C \approx -\alpha_F I_E$$

analogously, the reverse gain current α_R can be defined by considering this analysis in the reverse mode region.

The discussion is concluded by introducing two more parameter, which are the well know forward common-emitter current gain β_F and the reverse common-emitter current gain β_R:

$$\beta_F = \frac{\alpha_F}{1 - \alpha_F}$$
$$\beta_R = \frac{\alpha_R}{1 - \alpha_R} \tag{1.5}$$

1.1.3 From the BJT to the HBT.

Up to now, the conventional BJT has been discussed, it is now introduced the Heterojunction Bipolar Transistor.

In 1.1.2 , it was shown that it is possible to optimize the transport factor α_T by imposing the condition of having a base length smaller than the diffusion base length or equivalently, by

making the transit time of minority carriers in the base much smaller than the carrier's lifetime; moreover epitaxial growth allows for a further reduction of the base width to the nanometer scale, whereas in order to optimize the emitter efficiency one needs to impose the condition of having higher doping on the emitter side with respect that of the base region [3], [2].

Indeed, assuming the presence of a difference in the energy gaps between the emitter and base regions, denoted as $\Delta E_g = E_{gE} - E_{gB}$, it can be demonstrated that the emitter efficiency is given by the eq.(1.6) [3]:

$$\gamma = \left[1 + \frac{N_B w_B D_{pE} N_{vE} N_{cE}}{N_E x_E D_{nB} N_{vB} N_{cE}} e^{-\Delta E_g / k_B T}\right]^{-1} \tag{1.6}$$

where N_{vE} and N_{cE} represent the effective densities of states in the valence and conduction bands of the emitter, respectively, while N_{vB} and N_{cB} refer to the corresponding densities in the base. In a typical BJT, $\Delta E_g = 0$ and $N_{jE} = N_{jB}$ for $j = v, c$. Given that $D_{pB} \approx D_{nE}$ and $W_B < x_E$, varying ΔE_g is the only effective method to maximize γ.

Assuming $\alpha_T \approx 1$ and incorporating the Einstein relation, the common-emitter current gain can be approximated as eq.(1.7) [3]:

$$\beta_F \approx \left(\frac{\mu_{nB} x_E N_{vB} N_{cB}}{\mu_{pE} w_B N_{vE} N_{cB}}\right) \frac{N_E}{N_B} e^{-\Delta E_g / k_B T} \tag{1.7}$$

As it is known, two important figure of merits which provide a characterization of a transistor are the cut-off frequency and the maximum oscillation frequency.

The Heterojunction Bipolar Transistor allows for the overcoming of a number of limitations that arise once one considers using the homojunction BJT whose cut-off frequency is greater than few GHz. Indeed, in the case of homojunction BJT, once the doping level of the emitter leads to the so-called bandgap narrowing effect [4], [5] which is, the material gap is slightly decreased by the high level of doping according to the formula (1.8), which is known as the Lanyon-Tuft model [6], [7],

$$\Delta E_{gE} = \frac{3q^2}{16\pi\varepsilon_r^{1.5}} \sqrt{\frac{N_{kE}}{k_B T}} \tag{1.8}$$

where ε_r is the permittivity of the semiconductor and ΔE_{gE} is the decrease in the energy gap at the emitter and N_{kE} is the donor or acceptor doping at the emitter. It is evident that a slight narrowing of the bandgap has a significant detrimental effect on the common-emitter current. Additionally, it is important to consider another notable effect arising from the condition $N_E \gg N_B$, meaning that the homojunction BJT experiences a higher input base resistance, which in turn leads to a reduction in the device's maximum oscillation frequency.

In the case of the HBT, where a smaller bandgap can be used for the base compared to the emitter, the condition [3]

$$\frac{N_B}{N_E} e^{-\Delta E_g / k_B T} \ll 1$$

can be satisfied by appropriately selecting ΔE_g, even when $N_E \approx N_B$. This allows for the design of transistors with reduced base resistance, thereby increasing the maximum frequency f_{max}.

The improvement in emitter efficiency can be interpreted as a modification in the barrier potential that resists hole diffusion from the base into the emitter. In fact, the overall effect of the heterojunction is governed by the energy gap difference, which also influences the intrinsic carrier concentration.

2.Description of the BJT equivalent models

In this chapter, the Ebers-Moll and Gummel-Poon model are presented. These two models will be descripted, and their differences will be pointed out. In particular the first paragraph of this chapter will describe the Ebers-Moll model whereas in the second one, the Gummel-poon will be shown. This chapter is largely inspired from [1] and it will closely follow the presentation given in [1].

2.1.Ebers-Moll Model of a BJT.

In this paragraph, the two versions of the Ebers-Moll model [1], [8], [9] are presented, and the equivalence of these two is discussed. Then the large-signal model is also presented.

2.1.1.Static Model

The idea behind the Ebers-Moll model is to describe the BJT as a pair of diodes working together and it express this idea by means of formal equation.

There are two version of the Ebers-Moll model: the first one is called the injection version and the second one the transport version [9], [1]. These versions are mathematically the same; but the second one is preferred when it comes down to computer simulation.

Let the discussion begin with the static injection version whose circuital representation is given in Fig. 5

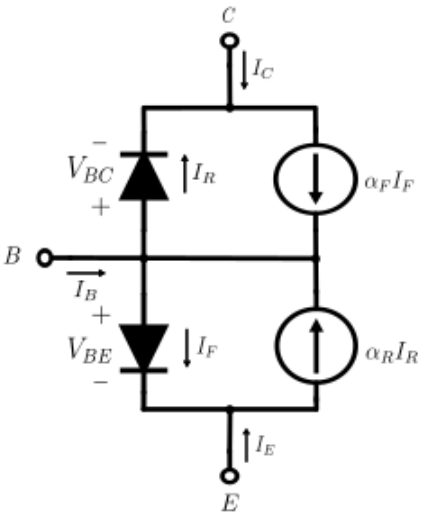

Fig. 5 Static Injection Version

The reference currents are I_F and I_R , the currents that are flowing through the diodes. Thus, it can be written [1], [9]

$$I_F = I_{ES}\left(e^{qV_{BE}/kT} - 1\right) \tag{2.9}$$

$$I_R = I_{CS}\left(e^{qV_{BC}/kT} - 1\right) \tag{2.10}$$

Where I_{ES} and I_{CS} are the base-emitter and the base-collector saturation currents, respectively.

It is easy to see from the schematic in Fig. 5 that the following relations hold [9], [1]:

$$\begin{aligned} I_C &= \alpha_F I_F - I_R \\ I_E &= -I_F + \alpha_R I_R \\ I_B &= (1-\alpha_F) I_F + (1-\alpha_R) I_R \end{aligned} \tag{2.11}$$

where α_F and α_R are the forward and reverse current gains of BJT, defined in chapter 1.1.2 .

A justification for such model may be given as follows: The two diodes are representing the BJT base-emitter and base-collector junctions. I_F(respectively, I_R) is the current that would flow across the base-emitter region for a given V_{BE}(respectively, V_{BC}) if the collector (emitter) region is seen as an ohmic contact which does not interfere with the base [1], [9]. Regarding the two current-dependent current sources, they are representing the physical phenomenon which couples the two junctions in the base region [1].

From the equations (2.11), it follows that this model is fully described by four parameters, and if one takes into account also the reciprocity property, they can be reduced up to three parameters [1]. Indeed, such property gives

$$\alpha_F I_{ES} = \alpha_R I_{CS} \equiv I_S \tag{2.12}$$

where I_S is the saturation current of the BJT [1].

Finally, let one consider the transport model, shown in Fig. 5, where the reference currents are I_{CC} and I_{EC} are those flowing the model's current sources and are given by [1]

$$I_{CC} = I_S\left(e^{qV_{BE}/kT} - 1\right) \tag{2.13}$$

$$I_{EC} = I_S\left(e^{qV_{BC}/kT} - 1\right) \tag{2.14}$$

As it was done before, the terminal currents can be computed and they are given by [1], [9], [8]

$$
\begin{aligned}
I_C &= I_{CC} - \frac{I_{EC}}{\alpha_R} \\
I_E &= -\frac{I_{CC}}{\alpha_F} + I_{EC} \\
I_B &= \left(\frac{1}{\alpha_F} - 1\right) I_{CC} + \left(\frac{1}{\alpha_R} - 1\right) I_{EC}
\end{aligned}
\tag{2.15}
$$

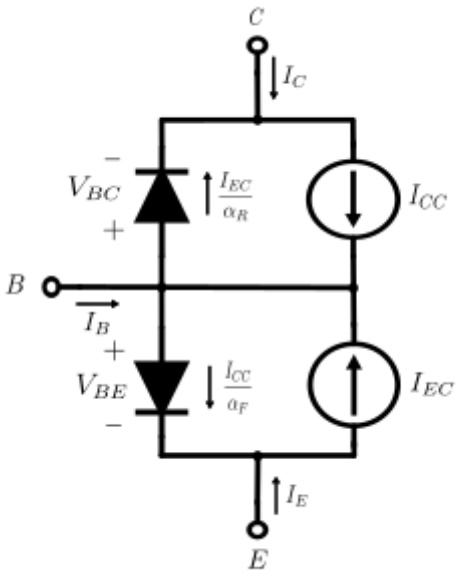

Fig. 6 Static Transport Version.

Now, a change of the topology can be made, as shown in Fig. 7 . Indeed, one can replace the two reference current sources with a single current source (I_{CT}) between the emitter and the collector, defined by the expression [9], [1]

$$I_{CT} = I_{CC} - I_{EC} = I_S\left(e^{qV_{BE}/kT} - e^{qV_{BC}/kT}\right) \tag{2.16}$$

This last equation allows for a change in the equation for the diode saturation currents, and those equations are now written as [1]

$$\frac{I_{CC}}{\beta_F} = \frac{I_S}{\beta_F}\left(e^{qV_{BE}/kT} - 1\right) \tag{2.17}$$

$$\frac{I_{EC}}{\beta_R} = \frac{I_S}{\beta_R}\left(e^{qV_{BC}/kT} - 1\right) \tag{2.18}$$

where β_F and β_R have been defined in eq.(1.5)

Referring to Fig. 7, the BJT's terminal currents can be computed, and by doing so one obtains [1]:

$$
\begin{aligned}
I_C &= I_{CT} - \frac{I_{EC}}{\beta_R} \\
I_E &= -\frac{I_{CC}}{\beta_F} - I_{CT} \\
I_B &= \frac{I_{CC}}{\beta_F} + \frac{I_{EC}}{\beta_R}
\end{aligned}
\tag{2.19}
$$

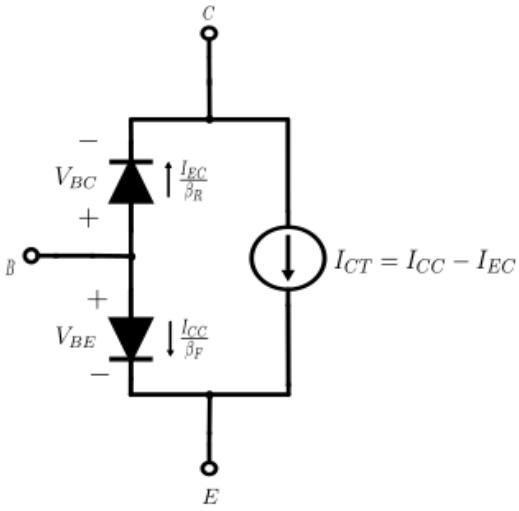

Fig. 7 modified topology of the Trasport version.

Up to now only the ideal case of the Erbes-Moll have been dealt with, but in order to have a model which can give as good simulation results, one needs to take in to account some others effects [1]. In particular, one needs to take into account the effects due to [1]:

1. The presence of parasitic base, collector and emitter resistance
2. The dependence of I_S on V_{BC} which leads to the so-called base-width modulation effects or Early effect. A more accurate description of this effect will be given by the Gummel-Poon model

The first point is presented.

By introducing the three parasitic resistances one aims to improve the dc characterization of our model. The three resistances are representing the ohmic resistances in the active region that are seen from the base, collector and emitter, respectively [1].

The equivalent circuit is shown in Fig. 8 .

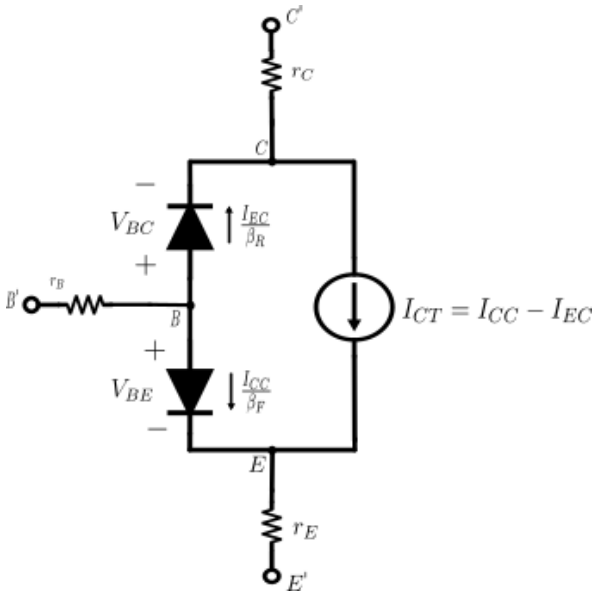

Fig. 8 Transport model with the parasitic resistances.

The resistance r_C has two main effects: the first of those is to decrease the slope of the curves in the saturated region for low collector-emitter voltages; the other one is the fact that such resistance limits the current-handling capability of the BJT and also it limits the maximum operating frequency of the BJT itself at high current [1].

Regarding the emitter resistance r_E, since the emitter is the most heavily doped region in order to produce a high β_F one has that the dominant component of such resistance is in the contact region and due to its low value (typically around 1Ω) it is often neglected [1].

However, its main effect is to reduce the voltage seen by the emitter-base junction by a factor of $r_E I_E$; this effect may be seen from a different perspective, indeed its effect on V_{BE} is the same as having an equivalent resistance on the base whose value is $(1 + \beta_F) r_E$, and this, in turn, implies that the base current and therefore the collector current are affected by r_E [1]. Moreover, it may introduce a non-negligible error on the measurement of r_B [1].

Finally, the base resistance r_B is considered; the main impact of this resistance is its effect on the small-signal model and in the transient responses. It is worth noticing that it is the most difficult parameter to be measured. The difficult in its measurement is in part due to, as described earlier, the effect of the emitter resistance and in part due to the dependence of such resistance on the operating point [1].

After the brief discussion about the parasitic resistances, one starts tackling the base-width modulation effect or the Early effect.

This effect consists in a variation of the base width, W_B, which in turn is the result of a variation in the collector-base junction voltage. When the BJT is in its normal region, the collector-base junction is forward-biased and the emitter-base junction is reverse-biased. It is known that the width of the depletion region of p-n junction is strongly dependent on the applied voltage, and therefore a large variation in V_{BC} will lead to a significant variation of the collector-base depletion region eventually resulting into a thin base width [1]. As final result the early effect

affects mainly the saturation current I_S , the forward gain current β_F and the forward transient time τ_F by means of the base transient time τ_{BF} [1].

For describing this effect, a new parameter is used, and it is the so-called Early voltage, V_A, in the active region of the BJT.

The analysis to the define such parameter assumes that the BJT is working in the linear region, then it determines the effect of base-width modulation on the base width and then it finds the three parameters related to the base width. Once the analysis completed, one obtains the following results [1], [9]:

$$W_B(V_{BC}) = W_{B0}\left(1 + \frac{V_{BC}}{V_A}\right) \tag{2.20}$$

$$I_S(V_{BC}) = \frac{I_{S0}}{1 + \frac{V_{BC}}{V_A}} \approx I_{S0}\left(1 - \frac{V_{BC}}{V_A}\right) \tag{2.21}$$

$$\beta_F(V_{BC}) = \frac{\beta_{F0}}{1 + \frac{V_{BC}}{V_A}} \approx \beta_{F0}\left(1 - \frac{V_{BC}}{V_A}\right) \tag{2.22}$$

$$\tau_{BF}(V_{BC}) = \tau_{BF0}\left(1 + \frac{V_{BC}}{V_A}\right)^2 \tag{2.23}$$

where the V_A is defined as follows [1]:

for a NPN,

$$V_A = \left(\frac{1}{W_{B0}}\frac{dW_B(V_{BC})}{dV_{BC}}\bigg|_{V_{BC}=0}\right)^{-1} \tag{2.24.1}$$

for a PNP,

$$V_A = \left(-\frac{1}{W_{B0}}\frac{dW_B(V_{BC})}{dV_{BC}}\bigg|_{V_{BC}=0}\right)^{-1} \tag{2.24.2}$$

where I_{S0}, β_{F0} and τ_{BF0} are the values of the parameters for $V_{BC} = 0$ [1].

Looking at the formulas from $(2.19)$to (2.23) the following considerations can be made.

First as equation $(2.24.1)$ and $(2.24.2)$ are suggesting, the difference between a PNP and a NPN lies uniquely on the opposite sign of V_{BC}, thus considering a NPN in which V_{BC} is negative, since the collector-base junction has to be reverse-biased, it can be seen that an increase in V_{BC} leads to an increase in the base width and to a positive sign. The role of the minus sign in eq.$(2.24.2)$ is used to preserve V_A as a positive quantity for a NPN BJT [1], [9].

With the exception of τ_{BF}, which will be described later on, I_S and β_F are accounting for the base width modulation. If the transport model is used, the following equation are obtained

$$I_{CT} = \frac{I_{S0}}{1 + V_{BC}/V_A}\left(e^{qV_{BE}/kT} - e^{qV_{BC}/kT}\right) \quad (2.25)$$

$$I_B = \frac{I_{S0}}{\beta_{F0}}\left(e^{qV_{BE}/kT} - 1\right) + \frac{I_{S0}}{\beta_R}\left(e^{qV_{BC}/kT} - 1\right) \quad (2.26)$$

where the first term of the left-hand side in eq.(2.25) the dependence on V_A has been canceled out, since both I_S and β_F are depending on it [1], [9]. Moreover, the second term is negligible in the active region, and so one finds that I_B is independent of the Early effect [1], [9].

2.1.2. Ebers-Moll Large-Signal Model

In order to model the large-signal behavior of the BJT one needs to consider the charge-storge effects of the device. Indeed, if these effects are not accounted for, the device would be infinitely fast due to the absence of charge storage, and the currents could be charged in zero time [1], [9].

The charge storage of a BJT is model by means of three types of capacitors: two non-linear junction capacitors, two non-linear diffusion capacitor and a constant substrate capacitor [1], [9].

The diffusion capacitances are used to model the mobile carriers in the BJT. This charge is composed of two main contributions: one contribution is due to the reference collector current source, I_{CC}, and the other is due to the reference emitter current source I_{EC} and each contribution is modeled as a capacitor [1], [9].

Below in figure 5 is given the schematic of the equivalent model.

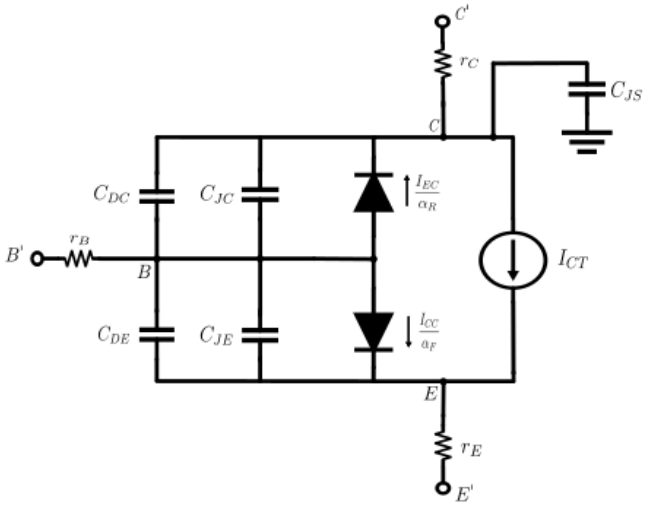

Fig. 9 Large Signal Ebers-Moll model.

In order to evaluate the capacitance that is associated with the I_{CC} the total mobile charge needs to be taken into account, and so one needs to assume that the emitter-base junction is forward-biased and $V_{BC} = 0$ [1], [9].

If our analysis is reduced to the one-dimensional case of constant base doping with negligible base recombination and low-level injection in the BJT the main contribution to the total charge might be identified and it can be written as [1], [9]:

$$Q_{DE} = Q_E + Q_{JE} + Q_{BF} + Q_{JC} \tag{2.27}$$

where one called:

- Q_E the mobile minority charge in the neutral emitter region
- Q_{JE} the mobile minority charge in the emitter-base depletion region associated with I_{CC}
- Q_{BF} the mobile minority charge in the neutral base region
- Q_{JC} the mobile minority charge in the base-collector depletion region associated with I_{CC}

Then, by the neutrality charge property, there will be an equal amount of majority charges stored in the neutral region.

The eq.(2.27) may be rewritten as follows, once one considers the delays and transits times of each region [1], [9]

$$Q_{DE} = (\tau_E + \tau_{EB} + \tau_{BF} + \tau_{CB})I_{CC} \equiv \tau_F I_{CC} \tag{2.28}$$

where one called:

- τ_E the emitter delay
- τ_{EB} the emitter-base depletion region transit time
- τ_{BF} the base transit time
- τ_{CB} the base-collector depletion region
- τ_F the total forward transit time.

Analogously the total charge Q_{DC} can be defined, associated to I_{EC} and to the relatives delays and transit times, τ_R indicates the total reverse transit time [1], [9].

If the BJT operates in the saturated mode, that is V_{BE} and V_{BC} are both forward-biased, both Q_{DE} and Q_{DC} are modeled by two nonlinear capacitors [1], [9]

$$C_{DE} \equiv \frac{dQ_{DE}}{dV_{BE}} = \frac{d(\tau_F I_{CC})}{dV_{BE}}$$
$$C_{DC} \equiv \frac{dQ_{DC}}{dV_{BC}} = \frac{d(\tau_R I_{EC})}{dV_{BC}} \tag{2.29}$$

Regarding the two constant capacitances of the substrate, those model the fixed charges which are stored in the depletion regions. Called Q_{JE} and Q_{JC} these charges one can define the associated capacitances C_{JE} and C_{JC} which are dependent on the bias voltage of the junctions, and are defined as [1], [9]

$$C_{JE}(V_{BE}) = \frac{C_{JE0}}{\left(1 - V_{BE}/V_{JE}\right)^{m_E}}$$
$$C_{JC}(V_{BC}) = \frac{C_{JC0}}{\left(1 - V_{BC}/V_{JC}\right)^{m_C}} \tag{2.30}$$

where C_{JE0} and C_{JC0} are the values of the emitter-base and collector-base junction capacitances at $V_{BE} = 0$ or $V_{BC} = 0$, V_{JE} and V_{JC} are the emitter-base and collector-base barrier potentials, and m_E and m_C are the emitter-base and collector-base capacitance gradient factor [1], [9].

From the definition of capacitance, it can be naturally derived the amount of charge stored in such capacitance as result of a simple integration, therefore obtaining [1], [9]:

$$Q_{JE} = \int_0^{V_{BE}} C_{JE}(V)dV = \frac{C_{JE0}}{1 - m_E}\left(1 - \frac{V_{BE}}{V_{JE}}\right)^{1-m_E}$$
$$Q_{JC} = \int_0^{V_{BC}} C_{JC}(V)dV = \frac{C_{JC0}}{1 - m_C}\left(1 - \frac{V_{BC}}{V_{JC}}\right)^{1-m_C} \tag{2.31}$$

One should notice, however, that for $V_{BE} = V_{JE}$ or $V_{BC} = V_{JC}$ the equation predicts a divergent value for the capacitances. As shown by Chawa and Gummel [10], [1] this is due to the fact that under forward-bias condition, it is no longer true that the transit time in the depletion region can be consider arbitrarily small. In such condition than the model has to be changed so that this effect is taken into account, and the equation (which has to be specialized to the case of C_{JE} and C_{JC}) is given by

$$C_J = 2^m C_{J0}\left[2m\frac{V}{V_J} - (1 - m)\right] \tag{2.32}$$

when $V \geq V_J/2$, in this way the infinite value of the capacitances is being avoided.

Before directing our attention to the Gummel-Poon model a list of important formulas is given, which are used in order to model correctly the behavior of the BJT, moreover these formulae [1], [9] will be needed when the thermal effects will be taken into account.

$$Q_{BE} = \begin{cases} \tau_F I_{CC} + C_{JE0}\int_0^{V_{BE}}\left(1 - \frac{V}{V_{JE}}\right)^{-m_E} dV, & V_{BE} < FC \times V_{JE} \\ \tau_F I_{CC} + C_{JE0}F_1 + \frac{C_{JC0}}{F_2}\int_{FC\times V_{JE}}^{V_{BE}}\left(F_3 + \frac{m_E V}{V_{JE}}\right)dV, & V_{BE} \geq FC \times V_{JE} \end{cases} \tag{2.33}$$

$$Q_{BC} = \begin{cases} \tau_R I_{EC} + C_{JC0} \int_0^{V_{BC}} \left(1 - \frac{V}{V_{JC}}\right)^{-m_C} dV, & V_{BC} < FC \times V_{JC} \\ \tau_R I_{EC} + C_{JC0} F_1 + \frac{C_{JC0}}{F_2} \int_{FC \times V_{JC}}^{V_{BC}} \left(F_3 + \frac{m_C V}{V_{JC}}\right) dV, & V_{BC} \geq FC \times V_{JC} \end{cases} \tag{2.34}$$

where $Q_{BE} = Q_{DE} + Q_{JE}$ and $Q_{BC} = Q_{DC} + Q_{JC}$

$$Q_{CS} = \begin{cases} C_{JS0} \int_0^{V_{CS}} \left(1 - \frac{V}{V_{JS}}\right)^{-m_s} dV\ , & V_{CS} < 0 \\ C_{JS0} \int_0^{V_{CS}} \left(1 + \frac{m_S V}{V_{JS}}\right) dV\ , & V_{CS} \geq 0 \end{cases} \tag{2.35}$$

Or equivalently, one has

$$C_{BE} = \frac{dQ_{BE}}{dV_{BE}} = \begin{cases} \tau_F \frac{dI_{CC}}{dV_{BE}} + C_{JE0} \left(1 - \frac{V_{BE}}{V_{JE}}\right)^{-m_E} & V_{BE} < FC \times V_{JE} \\ \tau_F \frac{dI_{CC}}{dV_{BE}} + \frac{C_{JE0}}{F_2} \left(F_3 + \frac{m_E V_{BE}}{V_{JE}}\right) & V_{BE} \geq FC \times V_{JE} \end{cases} \tag{2.36}$$

$$C_{BC} = \frac{dQ_{BC}}{dV_{BC}} = \begin{cases} \tau_R \frac{dI_{EC}}{dV_{BC}} + C_{JC0} \left(1 - \frac{V_{BC}}{V_{JC}}\right)^{-m_C} & V_{BC} < FC \times V_{JC} \\ \tau_R \frac{dI_{EC}}{dV_{BC}} + \frac{C_{JC0}}{F_2} \left(F_3 + \frac{m_C V_{BC}}{V_{JC}}\right) & V_{BC} \geq FC \times V_{JC} \end{cases} \tag{2.37}$$

$$C_{CS} = \begin{cases} C_{JS0} \left(1 - \frac{V_{CS}}{V_{JS}}\right)^{-m_S} & V_{CS} < 0 \\ C_{JS0} \left(1 + \frac{m_S V_{CS}}{V_{JS}}\right) & V_{CS} \geq 0 \end{cases} \tag{2.38}$$

where, for the base-emitter junction one defines

$$F_1 = \frac{V_{JE}}{1 - m_E}[1 - (1 - FC)^{1-m_E}]$$

$$F_2 = (1 - FC)^{1+m_E} \tag{2.39}$$

$$F_3 = 1 - FC(1 + m_E)$$

and for the base collector junction

$$F_1 = \frac{V_{JC}}{1 - m_E}[1 - (1 - FC)^{1-m_C}]$$

$$F_2 = (1 - FC)^{1+m_C} \tag{2.40}$$

$$F_3 = 1 - FC(1 + m_C)$$

The factor FC takes values in the range from 0 to 1, and it used to compute the voltage in the forward-bias region, beyond which the capacitance is modelled by means of a linear extrapolation. [1], [9]. The default value of such factor is 0.5. [1], [9].

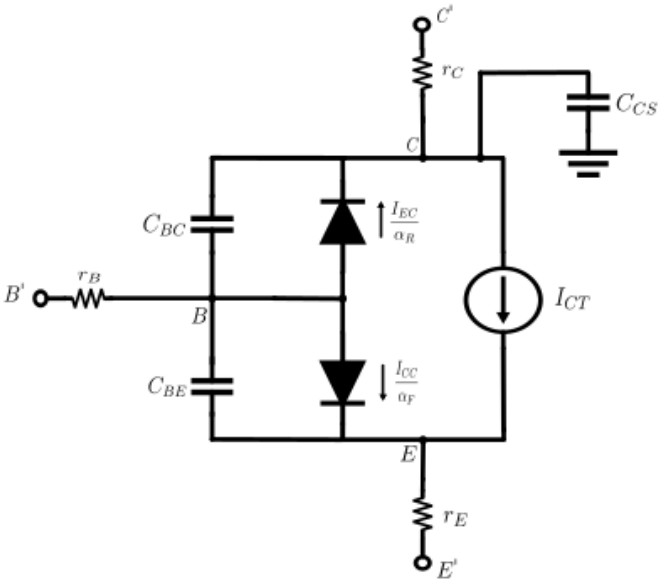

Fig. 10 Large Signal Erbes-Moll model with C_{BE} and C_{BC}

2.1.3. Erbes-Moll Small-Signal

As usual in order to find the small signal model, one linearizes the large signal model of the BJT. In order to do so, a quiescent point Q is selected then the Taylor expansion is performed around that point; such quiescent point is chosen inside the active region of the BJT [1], [9].

Since it is assumed to work in active mode, the relation between the collector current and base-emitter voltage is given by [1], [9]

$$I_C = I_S e^{qV_{BE}/kT} \tag{2.41}$$

Hence, one computes the variation of I_C over the variation of V_{BE} which yields

$$\left.\frac{dI_{CC}}{dV_{BE}}\right|_Q = \frac{qI_S}{kT} e^{qV_{BE}/kT} = \left.\frac{qI_C}{kT}\right|_Q \equiv g_{mF} \tag{2.42}$$

which is the familiar transconductance of the BJT [1], [9]. Repeating these steps over the various equation one has seen so far; the following results are obtained by the ratio between the variation of I_B and the variation of V_{BE}, one gets

$$g_\pi = \left.\frac{dI_B}{dV_{BE}}\right|_Q = \frac{g_{mF}}{\beta_F} \tag{2.43}$$

which means one has a resistor, $r_\pi = 1/g_\pi$, from base to emitter [1], [9].

From the ratio between the variation of I_C and the variation of V_{BC} one gets [1], [9]

$$\left.\frac{dI_C}{dV_{BC}}\right|_Q = \left.\frac{I_C}{|V_A|}\right|_Q = \frac{g_{mF}kT}{q|V_A|} \equiv g_0 \tag{2.44}$$

Moreover, the variation in V_{BC} results in a variation of the I_B which means that this effect can be model as a resistance r_μ from collector to base, and if V_{BE} is assumed to be constant then, it can be written

$$\left.\frac{dI_B}{dV_{BC}}\right|_Q = \left.\frac{d(I_C/\beta_R)}{dV_{BC}}\right|_Q = \frac{g_{mR}}{\beta_R} \tag{2.45}$$

in addition, one needs to take into account base resistance, indeed the Current-crowding effect has to be considered which causes an overall dc base resistance that depends on the collector current [1]. However, the Erbes-Moll model does not naturally account for this effect so one needs to add the following conductance:

$$g_x = \frac{1}{r_B} \tag{2.46}$$

In this way the nonlinear capacitance, viewed before, can be also linearized and a leap to the final results is made, which will be relevant once one considers the thermal effects [1], [9].

$$C_\pi \equiv C_{BE} = \begin{cases} \tau_F \dfrac{qI_S}{kT} e^{qV_{BE}/kT} + C_{JE0}\left(1 - \dfrac{V_{BE}}{V_{JE}}\right)^{-m_E} & V_{BE} < FC \times V_{JE} \\ \tau_F \dfrac{qI_S}{kT} e^{qV_{BE}/kT} + \dfrac{C_{JE0}}{F_2}\left(F_3 + \dfrac{m_E V_{BE}}{V_{JE}}\right) & V_{BE} \geq FC \times V_{JE} \end{cases} \tag{2.47}$$

$$C_{\mu} \equiv C_{BC} = \begin{cases} \tau_R \frac{qI_S}{kT} e^{qV_{BC}/kT} + C_{JE0}\left(1 - \frac{V_{BC}}{V_{JC}}\right)^{-m_C} & V_{BC} < FC \times V_{JC} \\ \tau_R \frac{qI_S}{kT} e^{qV_{BC}/kT} + \frac{C_{JC0}}{F_2}\left(F_3 + \frac{m_C V_{BC}}{V_{JC}}\right) & V_{BC} \geq FC \times V_{JC} \end{cases} \quad (2.48)$$

$$C_{CS} = \begin{cases} C_{JS0}\left(1 - \frac{V_{CS}}{V_{JS}}\right)^{-m_S} & V_{CS} < 0 \\ C_{JS0}\left(1 + \frac{m_S V_{CS}}{V_{JS}}\right) & V_{CS} \geq 0 \end{cases} \quad (2.49)$$

where F_1, F_2, F_3 are the same one that were defined for the large-signal model [1].

2.2.Gummel-Poon Model.

The Gummel-Poon model can be viewed as an enhanced version of the Ebers-Moll model. As will be discussed in detail later, it incorporates three major effects of interest [1]. The first effect is the reduction in β at low currents, which describes the decline in current gain in the low-current section [1]. The second effect modeled is base-width modulation, and finally, the third effect is high-level injection [1].

2.2.1. Static Model

Now that the Ebers-Moll model has been discussed, it is time to focus on the Gummel-Poon model. As previously mentioned, it is essential to consider several significant second-order effects that are present in real devices. The two most important effects are low-current and high-current injection. The first effect results from a supplementary current in the base due to recombination, which impairs the current gain [1]. The second effect also reduces the current gain, while simultaneously causing an increase in τ_F and τ_R[1].

The variation of gain current with respect to current is the first to be discussed.

The recombination in the depletion region has the effect to modify the diode relationship in the junction current [1]. In order to model this effect, one needs to add four further parameters to Ebers-Moll Model seen until now [1]. The idea is to define the base current as a superposition of ideal diode e nonideal diode components, and these others components will be the one in charge of correctly modelling the static behavior of the β and will allow the introduction of the forementioned four parameters [1].

In general, there are three main sections of interest, see Fig. 11; The first section corresponds to low current values, where β increases as I_C increases, the second section encompasses the

intermediate current values, where β remains approximately constant as I_C continues to increase, and finally, the third section represents the high value current section, where β decreases as I_C increases [1].

An additional assumption is $V_{BC} = 0$ since one can approximate the behavior of β_F with respect of V_{BC} with eq.(2.22) for any non-zero value of V_{BC} [1]. Moreover, for simplicity, also β_F is

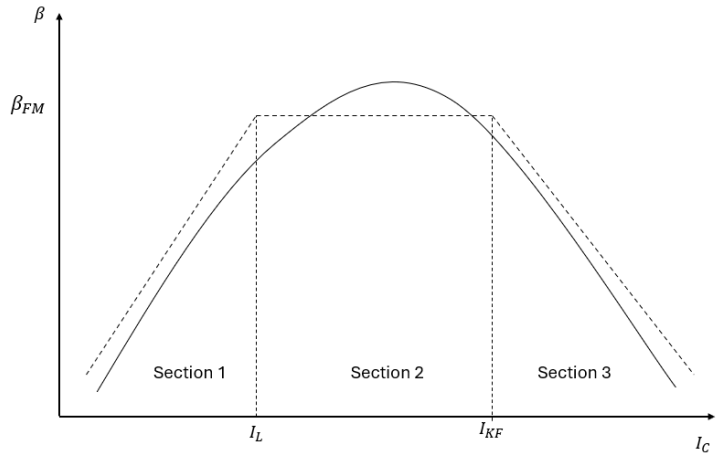

Fig. 11 Graph of β_F vs I_C

considered as function of I_C only [1]. A similar analysis may be conducted for β_R and for this reason it will be skipped.

The analysis of the behavior of β_F begins with the case [1], [9]:

I. Section 1 behavior of β_F for low intensity current.

As already mentioned, one witnesses a drop in β_F due to an additional component in the base current I_B [1], [9]. In the normal active region, three extra components to the current are caused by three factors: the first one is the recombination of carrier at the surface level; the second one is the recombination of the carrier that takes place in the emitter-base depletion region, and third one is the formation of channels in the emitter-base surface [1], [9].

The three components present a very similar variation with respect to V_{BE}, and these are to be added to the current I_B in the section 2, whose expression will be given later. Luckly enough the total expression can be simplified, and so getting the following expression:

$$I_B = I_{S,comp}\left(e^{qV_{BE}/n_{EL}kT} - 1\right) \qquad (2.50)$$

where n_{EL} is a nonideality factor called **non-ideal low-current base-emitter emission coefficient** whose value lies in the range between 1 and 4 and the value is typically obtained by fitting the curve [1], [9]. To make progress on the analytical front, it is the case that the recombination and channels that appear can be made negligible with careful processing, leading to the fact that the dominant component is given by the recombination that take place

in the emitter-base region, and normally $n_{EL} \approx 2$, and since $V_{BC} = 0$ is assumed, the base current takes the approximated form given by:

$$I_B = \frac{I_{S0}}{\beta_{FM0}}\left(e^{qV_{BE}/kT} - 1\right) + C_2 I_{S0}\left(e^{qV_{BE}/n_{EL}kT} - 1\right) \tag{2.51}$$

where one has that $I_{S,comp} = C_2 I_{S0}$ and the parameter I_{S0}, β_{FM0} will be defined in the section 2 [1], [9].

The new parameter C_2 is the **forward low-current non-ideal base current coefficient** [1], [9].

However, in general, in the active all of the three contributions will be present in the expression of I_B and such expression will be in general dependent on V_{BC} and so the complete expression for I_B is given as:

$$I_B = \frac{I_{S0}}{\beta_{FM0}}\left(e^{qV_{BE}/kT} - 1\right) + C_2 I_{S0}\left(e^{qV_{BE}/n_{EL}kT} - 1\right) + \\ + \frac{I_{S0}}{\beta_{RM}}\left(e^{qV_{BC}/kT} - 1\right) - C_4 I_{S0}\left(e^{qV_{BC}/n_{CL}kT} - 1\right) \tag{2.52.1}$$

and consequently, one also has

$$I_C = I_{S0}\left(e^{qV_{BE}/kT} - e^{qV_{BC}/kT}\right) - \frac{I_{S0}}{\beta_{RM}}\left(e^{qV_{BC}/kT} - 1\right) + \\ - C_4 I_{S0}\left(e^{qV_{BC}/n_{CL}kT} - 1\right) \tag{2.52.2}$$

where the new parameters n_{CL} and C_4 are the **non-ideal low-current base-collector emission coefficient** and the **reverse low-current non-ideal base current coefficient**, respectively [1], [9].

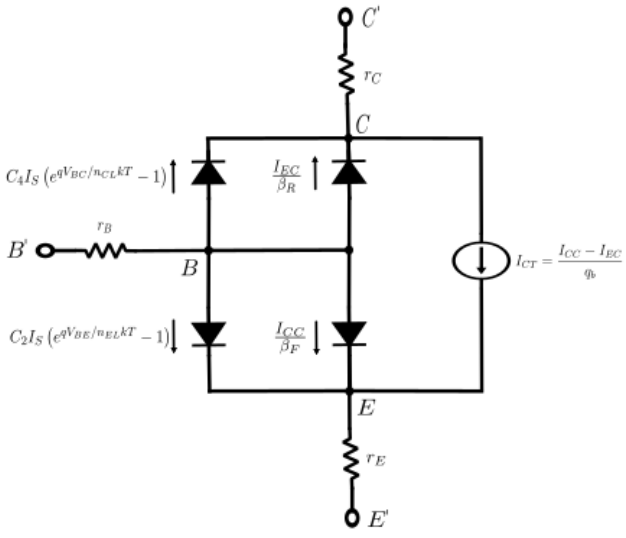

Fig.12 BJT Gummel-Poon static model as the new components of I_B are included

These supplementary contributions to I_B are represented by two non-ideal diodes incorporated into the Ebers-Moll model topology, as shown in Fig.12.

II. Section 2 behavior of β_F for intermediate intensity current.

In this region the Ebers-Moll model holds, and the β_F remains constant. In this region β_F is denoted as β_{FM} and in particular $\beta_{FM}(V_{BC} = 0) = \beta_{FM0}$, and the currents in this region are given by

$$I_C = I_{S0}(e^{qV_{BE}/kT} - 1)$$
$$I_B = \frac{I_{S0}}{\beta_{FM0}}\left(e^{qV_{BE}/kT} - 1\right) \quad (2.53)$$

and so, the two missing parameters in the low-current region are finally defined [1], [9].

III. Section 3 behavior of β_F for high intensity current.

To accurately describe and model the behavior of the BJT in this region, it is necessary to utilize the current density equation specific to the BJT. This equation is employed to determine the value of I_S and accounts for both the high-level injection effect and the base-width modulation effect [1], [9]. To achieve this, the analysis is performed under the assumption of one-dimensional conditions, and the objective is to express the DC current density for both electrons and holes in an NPN transistor [1], [9], [2].

To achieve this, it is assumed that the analysis is conducted in a one-dimensional framework, with the goal of formulating the DC current density for both electrons and holes in an NPN transistor [1], [9]. Those current densities are:

$$J_n = q\mu_n n(x)E(x) + qD_n\frac{dn(x)}{dx}$$
$$J_p = q\mu_p p(x)E(x) - qD_p\frac{dp(x)}{dx} \quad (2.54)$$

where $E(x)$ is the electric field, $n(x)$ is the free electron concentration and $p(x)$ is the free hole concentration [1], [9].

Typically, the emitter-base junction is designed to have high-injection efficiency. Moreover, in the active region, the collector-base junction is reversed-biased, so one must have a negligible flow of current across the region [1], [9]. In saturation or reverse mode, the collector-base region is forward-biased, however, it is assumed that the hole current flow is negligible which means $J_p \approx 0$ [1], [9].

From the second equation of (2.54) ,the electrical field can be derived:

$$E(x) = \frac{D_p}{\mu_p}\frac{1}{p(x)}\frac{dp(x)}{dx} \tag{2.55}$$

If this expression is substituted into the equation for J_n in (2.54), and after performing the calculations, the first equation in (2.54) becomes:

$$p(x)J_n = qD_n\frac{d}{dx}[p(x)n(x)] \tag{2.56}$$

if an integration is performed on both side inside the base region as indicated in Fig.13, therefore including the depletion region, and solving for J_n one finds [1], [9]

$$J_n = \frac{qD_n\big(n(x_C)p(x_C) - n(x_E)p(x_E)\big)}{\int_{x_E}^{x_C} p(x)dx} \tag{2.57}$$

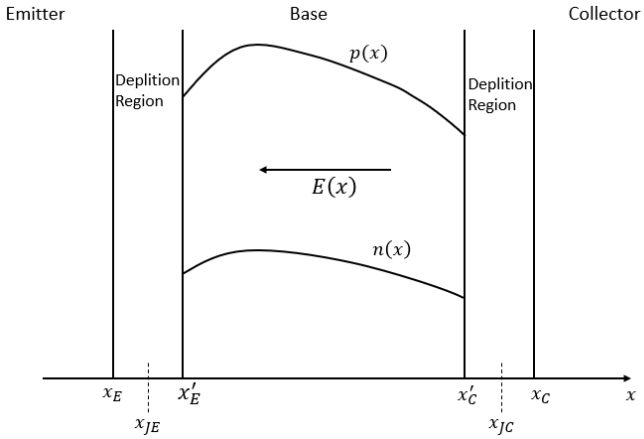

Fig.13 Base profile for the NPN transistor, specifying the integral limits.

recalling that [1], [9], [2]

$$\begin{aligned} n(x_C)p(x_C) &= n_i^2 e^{qV_{BC}/kT} \\ n(x_E)p(x_E) &= n_i^2 e^{qV_{BE}/kT} \end{aligned} \tag{2.58}$$

then J_n can be written as [1], [9]:

$$J_n = -\frac{qD_n n_i^2\left(e^{qV_{BE}/kT} - e^{qV_{BC}/kT}\right)}{\int_{x_E}^{x_C} p(x)}. \tag{2.59}$$

It is typically assumed that the depletion approximation is valid, which results in the integration region corresponding to the base region, as shown in Fig.13 [1], [9]. This leads to the following result:

$$I_n = -\frac{qD_n A_J n_i^2 \left[\left(e^{qV_{BE}/kT} - 1\right) - \left(e^{qV_{BC}/kT} - 1\right)\right]}{\int_{x'_E}^{x'_C} p(x)dx} \tag{2.60}$$

this is the total dc minority current along the positive x direction that results from the minority charges injected into the base at the emitter and/or collector and A_J is the emitter area [1], [9].

Comparing eq.(2.60) with eq.(2.16), at low-level injection i.e. $p(x) \approx N_A(x)$, leads to

$$I_S \approx \frac{qD_n A_J n_i^2}{\int_{x'_E}^{x'_C} N_A(x)dx} \tag{2.61}$$

However, it must be pointed out that originally the I_S was defined as a fundamental constant of the device, it is no longer a constant, so to resolve this inconsistency in the notation, for the Gummel-Poon model, the non-constant quantity I_{SS} is defined under low-current condition only [1], [9], [11].

Moreover, it has to be noticed that the x'_C and x'_E are function of an appropriate voltage since the depletion varies with the application of a voltage, then one defines the fundamental constant I_{SS} for $V_{BE} = 0$ and $V_{CB} = 0$ leading to [1], [9] :

$$I_{SS} = \frac{qD_n n_i^2 A_J}{\int_{x'_{C0}}^{x'_{E0}} N_A(x)\,dx} \tag{2.62}$$

Now the depletion approximation is relaxed, so the carriers in the depletion region are included, leading to

$$I_{SS} = \frac{qD_n n_i^2 A_J}{\int_{x_{E0}}^{x_{C0}} p_0(x)dx} \tag{2.63}$$

where $p_0(x)$ is the hole concentration in the neutral base at thermal equilibrium.

All of this was done to derive the behavior of the BJT in the high-current regime. The final step involves defining the total majority charge in the neutral base region, normalized with respect to its zero-bias value, in order to connect I_S to I_{SS} inside the expression of I_{CT} and to determine the collector current in the high-injection level regime [1], [9].

Called Q_B the total majority charge, it is defined as:

$$Q_B = \int_{x'_E}^{x'_C} qA_J p(x)dx \tag{2.64}$$

and the zero-bias majority base charge, Q_{B0}, is defined as

$$Q_{B0} = \int_{x_{E0}}^{x_{C0}} qA_J p_0(x)dx \approx \int_{x'_{E0}}^{x'_{C0}} qA_J N_A(x)dx \tag{2.65}$$

therefore, after some algebra

$$I_{CT} = \frac{I_{SS}}{q_b}\left[\left(e^{qV_{BE}/kT} - 1\right) - \left(e^{qV_{BC}/kT} - 1\right)\right] \tag{2.66}$$

where $q_b = Q_B/Q_{B0}$ [1], [9], [11].

Eq.(2.66) is the new equation introduced by the Gummel-Poon model, and it brings with it the new fundamental concept of the normalized majority charge in the base, q_b, since all of the Gummel-Poon model derivation is dependent on this quantity [1], [9], [11].

The value of q_b needs to be determined. To accomplish this, it is observed that q_b can be written as

$$q_b = 1 + \frac{C_{JE}}{Q_{B0}}V_{BE} + \frac{C_{JC}}{Q_{B0}}V_{BC} + \frac{\tau_{BF}}{Q_B}I_{CC}^{(1)} + \frac{\tau_{BR}}{Q_{B0}}I_{EC}^{(1)} \tag{2.67}$$

this equation can be expanded as [1], [9]

$$q_b = 1 + \underbrace{\frac{V_{BE}}{V_B}}_{q_e} + \underbrace{\frac{V_{BC}}{V_A}}_{q_c} + \underbrace{\frac{\tau_{BF}}{Q_{B0}}I_{SS}\frac{e^{qV_{BE}/kT} - 1}{q_b}}_{q_{bF}} + \underbrace{\frac{\tau_{BR}}{Q_{B0}}I_{SS}\frac{e^{qV_{BC}/kT} - 1}{q_b}}_{q_{bR}} \tag{2.68}$$

where:

- $V_B = Q_{B0}/C_{JE}$ is the reverse Early Voltage
- $V_A = Q_{B0}\ /\ C_{JC}$ is the forward Early Voltage
- $I_{CC}^{(1)} = \frac{I_{SS}}{q_b}\left(e^{qV_{BC}/kT} - 1\right)$
- $I_{EC}^{(1)} = \frac{I_{SS}}{q_b}\left(e^{qV_{BE}/kT} - 1\right)$

It should be noted that q_e and q_c are modelling the effects of the base-width modulation, meanwhile q_{bF} and q_{bR} are modelling the effects of high-level injection [1], [9]. In order to simplify the algebra, the following quantities are defined [1], [9]:

$$q_b = q_1 + \frac{q_2}{q_b} \tag{2.69}$$

where:

$$q_1 = 1 + q_e + q_c = 1 + \frac{V_{BE}}{V_B} + \frac{V_{BC}}{V_A}$$
$$q_2 = \frac{\tau_{BF} I_{SS}\left(e^{qV_{BE}/kT} - 1\right) + \tau_{BR} I_{SS}\left(e^{qV_{BC}/kT} - 1\right)}{Q_{B0}} \tag{2.70}$$

By definition, q_1 is equal to unity at zero bias, indicating that, under zero-bias conditions, the electrical base width is the same as the physical base width. When both junctions are forward-biased, the electrical width becomes larger than the physical width, resulting in q_1 being greater than one [1], [9]. Conversely, when both junctions are reverse-biased, q_1 is less than one [1], [9]. This behavior shows that q_1 effectively models the effects of base-width modulation [1], [9].

The q_2 term models the effects of high-level injection [1], [9]. Specifically, it accounts for the excess majority base charge resulting from injected minority carriers [1], [9]. This excess majority-carrier base charge becomes significant when the injected minority carriers are comparable to the majority-carrier charge under zero-bias conditions, which occurs during high-level injection [1], [9].

The quadratic equation, that follows from eq.(2.69), can be resolved

$$q_b^2 + q_b q_1 + q_2 = 0 \tag{2.71}$$

which results in

$$q_b = \frac{q_1}{2} + \sqrt{\left(\frac{q_1}{2}\right)^2 + q_2} \tag{2.72}$$

where the negative solution of q_b has been excluded since it is by definition greater than zero [1], [9].

From eq. (2.72) it follows that [1], [9]

$$q_b \approx q_1 \quad \text{if} \quad q_2 \ll \frac{q_1^2}{4} \ (\text{low} - \text{level injection})$$
$$q_b \approx \sqrt{q_2} \quad \text{if} \quad q_2 \gg \frac{q_1^2}{4} \ (\text{high} - \text{level injection}) \tag{2.73}$$

I. Solution for the High-level injection case

In the normal active region at high-injection levels, $q_b \approx \sqrt{q_2}$ [1], [9]. For simplicity it will be considered only the case $V_{BC} = 0$, i.e. $q_{bR} = 0$ [1], [9]. The extension of the result to nonzero q_{bR} will be made by analogy [1], [9].

For $q_{bR} = 0$, one has [1], [9]

$$q_b = \sqrt{q_2} \approx \sqrt{\frac{\tau_{BF} I_{SS}}{Q_{B0}} e^{qV_{BE}/kT}} = \sqrt{\frac{\tau_{BF} I_{SS}}{Q_{B0}}} e^{qV_{BE}/2kT} \tag{2.74}$$

Therefore, one can derive I_C ($I_C = I_{CC}$ in this case) [1], [9],

$$I_C = \frac{I_{SS}\left(e^{qV_{BE}/kT} - 1\right)}{\sqrt{\tau_{BF} I_{SS}/Q_{B0}}\, e^{qV_{BE}/2kT}} \approx \sqrt{\frac{Q_{B0} I_{SS}}{\tau_{BF}}}\, e^{qV_{BE}/2kT} \tag{2.75}$$

Thus

$$I_C \propto e^{qV_{BE}/2kT} \tag{2.76}$$

II. Approximation for the expression of q_2

Moreover, the expression for the coefficient $\sqrt{Q_{B0} I_{SS}/\tau_{BF}}$ can be further approximated by considering the characteristics of $\ln I_C$ vs. V_{BE} at the two extremes: high- and low-level injection. Specifically, the low-current asymptote is approximately given by the following expression ($q_e \approx q_c \approx 0$) [1], [9]:

$$I_C \approx I_{SS} e^{qV_{BE}/kT} \tag{2.77}$$

The high-current asymptote is given by eq.(2.75) [1], [9]. At the intersection of these two asymptotes defines the knee current I_{KF} and the knee voltage V_{KF} [1], [9]. From eq. (2.75) it follows

$$I_{KF} = \sqrt{\frac{Q_{B0} I_{SS}}{\tau_{BF}}}\, e^{qV_{KF}/2kT} \qquad (\text{high} - \text{level}) \tag{2.78}$$

while, one has from eq. (2.1.28) [1], [9]

$$I_{KF} = I_{SS} e^{qV_{KF}/kT} \ (\text{low} - \text{level}) \tag{2.79}$$

than it follows [1], [9]

$$I_{KF} = \frac{Q_{B0}}{\tau_{BF}} \tag{2.80}$$

and by performing a similar analysis in the inverse region one can define I_{KR}, the knee current for I_E versus V_{BC} in such region, as [1], [9]

$$I_{KR} = \frac{Q_{B0}}{\tau_{BR}} \tag{2.81}$$

Further knowledge of the Gummel-Poon Model can be gained by studying the asymptotic behavior of β_F with respect to I_C in the short-circuit condition. In such condition the gain is practically constant at a certain value β_F for all the collector current greater than I_L, and it falls off with a slop of $1 - 1/n_{EL}$ for the collector current lesser than I_L and eventually the gain will fall off with a slop of -1 once the collector current is greater than I_{KF} (see, Fig. 11) [1], [9]. And so, the equation of the breaking point for the low-current is found, that is [1], [9]

$$I_L = I_S (C_2 \beta_{FM})^{n_{EL}/(n_{EL}-1)} \tag{2.82}$$

III. Final expression of q_b

The complete solution of the eq.(2.71) is given by

$$q_b = \frac{q_1}{2} + \sqrt{\left(\frac{q_1}{2}\right)^2 + q_2} \tag{2.83}$$

where:

$$q_1 = 1 + \frac{V_{BE}}{V_B} + \frac{V_{BC}}{V_A}$$
$$q_2 = \frac{I_{SS}}{I_{KF}}\left(e^{qV_{BE}/kT} - 1\right) + \frac{I_{SS}}{I_{KR}}\left(e^{qV_{BC}/kT} - 1\right) \tag{2.84}$$

and all the parameters in the above expression (V_B, V_A, I_{SS}, I_{KF} and I_{KR}) are directly measurable from the plots of $\ln I_C$ vs. V_{BE} in the normal active region, from the plots of $\ln I_E$ vs. V_{BC} in the inverse region, from the characteristics I_C vs. V_{CE} and I_E vs. V_{CE} [1], [9]. Once these parameters are identified, the values of q_1 and q_2 can be easily determined, which in turn allows for the calculation of q_b.

It is a point of interest to model the current crowding, i.e. the dependence of the base resistance on the current. This resistance can be view as the result of the sum of two contributions from two separate resistance [1], [9]. One of these contributions comes from the external resistance r_B (extrinsic base resistance) which consists of the contact resistance and the sheet resistance of the external base region [1], [9]. The other one is the resistance r_{BM} of the internal base region (intrinsic base resistance), this resistance is function of the current and it is located in the region of the base that lies directly under the emitter. In particular the dependence on the current come from non-zero base-region resistivity which, as result, causes a non-uniform decreasing in the bias of the base-emitter junction [1], [9].

It can be shown that the total base resistance can be written as [1]

$$r_{BB'} = r_{BM} + 3(r_B - r_{BM})\left(\frac{\tan z - z}{z\tan^2 z}\right) \tag{2.85}$$

where r_{BM} is the minimum base resistance that occurs at high current, r_B is the base resistance at zero bias and z is a variable of base resistivity thermal voltage, and intrinsic base length. Due to the computational complexity in calculating z one makes use of approximation method where the $\cos z$ is represented by the first two terms in its McLaurin series, and therefore its value is:

$$z = -\frac{1 + \sqrt{1 + 144I_B/\pi^2 I_{rB}}}{(24/\pi^2)\sqrt{I_B/I_{rB}}} \tag{2.86}$$

where I_{rB} is the current that flows through the base resistance when its value is half of the minimum one [1], [9].

At last, one can write the equations for the base current and the collector current which will be later used to model the dc behavior of our BJT

$$I_B = I_{SE}\left(e^{qV_{BE}/n_{EL}kT} - 1\right) + I_{SC}\left(e^{qV_{BC}/n_{CL}kT} - 1\right) + \frac{I_{SS}}{\beta_F}\left(e^{qV_{BE}/n_FKT} - 1\right) + \frac{I_{SS}}{\beta_R}\left(e^{qV_{BC}/n_RkT} - 1\right)$$

$$I_C = \frac{I_{SS}}{q_b}\left(e^{qV_{BE}/n_FkT} - e^{qV_{BC}/n_RkT}\right) - I_{SE}\left(e^{qV_{BE}/n_{EL}kT} - 1\right) - \frac{I_{SS}}{\beta_R}\left(e^{qV_{BC}/n_RkT} - 1\right) \quad (2.87)$$

where $I_{SE} = C_2 I_{SS}$ and $I_{SC} = C_4 I_{SS}$ [1], [9].

Moreover, the following approximations can be done for the expression of q_1 and q_b [1]:

$$q_1 = \frac{1}{1 - \frac{V_{be}}{V_B} - \frac{V_{bc}}{V_A}} \quad (2.88)$$

and

$$q_b = \frac{q_1}{2}\left[1 + \sqrt{1 + 4q_2}\right] \quad (2.89)$$

2.2.2 Gummel-Poon Large-Signal and Small-Signal Model.

The nonlinear charge elements are the same of the Ebers-Moll model as it was seen before, however the fact that I_{EC} and I_{CC} are depending on I_{SS} and q_b has to be taken into account [1]. Moreover, the Gummel-Pool model considers also three more effects and those are [1], [9]:

- The Distributed base-collector capacitance
- The τ_F modulation, also called transit charge
- The Distributed Phenomenon in the base region, also known as excess phase.

One begins to discuss the Distributed base-collector capacitance.

In order to find a better approximation of the distributed resistance and capacitance network in the base-collector region, one makes a partition in two parts [1], [9]. So, a new parameter, which allows such partition, is defined and it will be denoted as X_{CJC} whose range is the intervale $[0,1]$ and it represents the ratio of the partitioning. Therefore, the capacitance $X_{CJC}C_{JC}$ is placed between the internal base node and the collector, whereas $\left(1 - X_{CJC}\right)C_{JC}$ is the capacitance from the external base to the collector, and finally C_{JC} is the total base-collector capacitance [1], [9]. This parameter plays an important role at high frequency [1].

In order to implement this, one makes use of the following relations:

$$Q_{BX} = \begin{cases} C_{JC0}(1 - X_{CJC}) \int_0^{V_{BX}} \left(1 - \frac{V}{V_{JC}}\right)^{-m_C} dV & \text{for } V_{BX} < FC \times V_{JC} \\ C_{JC0}(1 - X_{CJC}) F_1 + \frac{C_{JC0}(1 - X_{CJC})}{F_2} \int_{FC \times V_{JC}}^{V_{BX}} \left(F_3 + \frac{m_C V}{V_{JC}}\right) dV & \text{for } V_{BX} \geq FC \times V_{JC} \end{cases} \quad (2.90)$$

or equivalently one may use:

$$C_{JX} = \begin{cases} C_{JC0}(1 - X_{CJC}) \left(1 - \frac{V_{BX}}{V_{JC}}\right)^{-m_C} & \text{for } V_{BX} < FC \times V_{JC} \\ \frac{C_{JC0}(1 - X_{CJC})}{F_2} \left(F_3 + \frac{m_C V_{BX}}{V_{JC}}\right) & \text{for } V_{BX} \geq FC \times V_{JC} \end{cases} \quad (2.91)$$

where F_1, F_2 and F_3 are those defined in eq.$(1.2.14)$ [1], [9]

After having introduced these new elements, the model is show in Fig. 14 below, where for simplicity one denotes

$$\tilde{I}_{SE} = C_2 I_{SS}\left(e^{qV_{BE}/n_{EL}kT} - 1\right)$$
$$\tilde{I}_{SC} = C_4 I_{SS}\left(e^{qV_{BC}/n_{CL}kT} - 1\right) \quad (2.92)$$

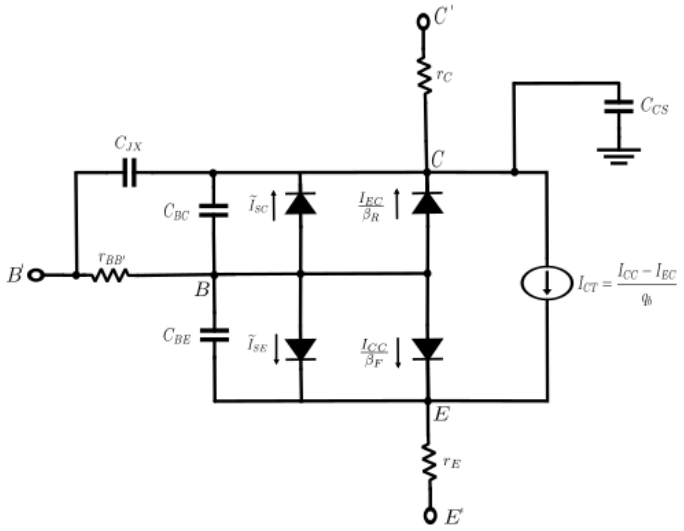

Fig. 14 Gummel-Poon Large-Signal Model with the distributed capacitance and the variable base resistance.

The expression for the capacitances C_{BE}, C_{BC} may be expressed in an explicit fashion, since the expression of I_{CC} and I_{EC} are known. Indeed, the following expressions are obtained:

$$C_{BE}(V_{BE}) = \begin{cases} \tau_F \dfrac{qI_{SS}}{n_F kT} e^{qV_{BE}/n_F kT} + C_{JE0}\left(1 - \dfrac{V_{BE}}{V_{JE}}\right)^{-m_E} & V_{BE} < FC \times V_{JE} \\ \tau_F \dfrac{qI_{SS}}{n_F kT} e^{qV_{BE}/n_F kT} + \dfrac{C_{JE0}}{F_2}\left(F_3 + \dfrac{m_E V_{BE}}{V_{JE}}\right) & V_{BE} > FC \times V_{JE} \end{cases} \tag{2.93}$$

$$C_{BC}(V_{BC}) = \begin{cases} \tau_R \dfrac{qI_{SS}}{n_R kT} e^{qV_{BC}/n_R kT} + X_{CJC} C_{JC0}\left(1 - \dfrac{V_{BC}}{V_{JE}}\right)^{-m_C} & V_{BC} < FC \times V_{JC} \\ \tau_R \dfrac{qI_{SS}}{n_R kT} e^{qV_{BC}/n_R kT} + \dfrac{C_{JC0}}{F_2}\left(F_3 + \dfrac{m_C V_{BC}}{V_{JC}}\right) & V_{BC} > FC \times V_{JC} \end{cases} \tag{2.94}$$

The next step in the list is the τ_F modulation or the transit charge.

The variation of τ_F at high collector currents is usually determined by means of empirical equation which establishes the relation between the gain-band-width product f_T and I_C for various V_{CE}, and one may divide the f_T vs. I_C in three domains [1].

At low currents, f_T is dominated by the junction capacitances and the forward transconductance g_{mF}, and since g_{mF} increases with the current so does f_T [1], [3].

At mid-current level f_T is at its maximum and is nearly constant; here the transit time is the time that the carriers need to traverse the base region and the collector depletion region [1]. Moreover, the emitter-base diffusion capacitance increases as the current increases, and as result of this it cancels out the increase in g_{mF}, eventually leading to a limit for f_T [1]. From these facts it follows that the maximum transit time is given by [1], [3], [9]

$$\tau_F = \frac{1}{2\pi f_T} \tag{2.95}$$

At high currents, f_T and then τ_F start to depend on I_C and V_{CE} and do not remain constant [1]. Physically, anomalies such as base push-out, lateral spreading, space-charge-limited current flow, and quasi-saturation increase the transit time and then decrease f_T [1], [9].

This effect is modeled by the following equation which is obtain empirically [1]:

$$ATF = 1 + X_{\tau F} e^{V_{BC}/1.44V_{\tau F}} \left(\frac{I_{CC}}{I_{CC} + I_{\tau F}}\right)^2 \tag{2.96}$$

This function multiplies τ_F in the charge equations. The constant value 1.44 represents the fact that when $V_{BC} = V_{\tau F}$ then the exponential has value equal to $^1/_2$. $X_{\tau F}$ is a parameter that controls the fall-off of f_T, $V_{\tau F}$ is a parameter that dominates the change of f_T vs. V_{CE} and lastly, the parameter $I_{\tau F}$ expresses how f_T changes with respect to the current [1].

It can be shown that [1]

$$f_T = \frac{1}{2\pi\tau_F\left[ATF + \frac{2(ATF-1)I_{\tau F}}{I_{CC}+I_{\tau F}} + \frac{kT}{q}n_F\frac{ATF-1}{1.44V_{\tau F}}\right]} \tag{2.97}$$

where it can be noticed that

$$\begin{aligned}\frac{dATF}{dI_{CC}} &= \frac{2(ATF-1)I_{\tau F}}{I_{CC}+I_{\tau F}} \\ \frac{dATF}{dV_{BC}} &= \frac{kT}{q}n_F\frac{ATF-1}{1.44V_{\tau F}}\end{aligned} \tag{2.98}$$

At low-current or high V_{CE} one has $ATF = 1$ and so the eq.(2.97)reduces to the familiar relation of the Ebers-Moll model given in eq.(2.95) [1].

When I_{CC} is large so that $I_{CC}/(I_{CC}+I_{\tau F}) \approx 1$ and V_{CE} is moderate the eq.(2.97). reduces to

$$f_T|_{I_C\to\infty} = \frac{1}{2\pi\tau_F\left[1 + X_{\tau F}\left(e^{V_{BC}/1.44V_{\tau F}} + qe^{\frac{V_{BC}}{1.44V_{\tau F}}}/n_F kT\cdot 1.44V_{\tau F}\right)\right]} \tag{2.99}$$

Thus, the high-current asymptote for a given V_{BC} is given by the parameters $X_{\tau F}$ and $V_{\tau F}$. Similarly, the asymptotic dependence of eq.(2.97)in the extremes of V_{BC} are:

$$f_T = \frac{1}{2\pi\tau_F[1 + X_{\tau F}(1 + q/n_F kT\cdot 1.44V_{\tau F})]} \quad \text{for } I_{CC}\to\infty, V_{BC}\to 0 \tag{2.100}$$

where

$$ATF \approx 1 + X_{\tau F} \text{ for } I_C\to\infty, V_{BC}\to 0 \tag{2.101}$$

Moreover,

$$f_T = \frac{1}{2\pi\tau_F} \text{ for } V_{BC}\to\infty \tag{2.102}$$

Thus, the maximum possible fall-off of f_T is, as said, controlled by $X_{\tau F}$.

This effect is expressed by the following expression for charge or equivalently the capacitance [1]

$$Q_{\tau FF} = \tau_{FF} \frac{I_{CC}}{q_b}$$
$$C_{\tau FF} = \frac{\partial Q_{\tau FF}}{\partial V_{BE}} \tag{2.103}$$

where τ_{FF} is the modulated transit time given by [1]

$$\tau_{FF} = \tau_F \left[1 + X_{\tau F} \left(\frac{I_{CC}}{I_{CC} + I_{\tau F}}\right)^2 e^{V_{BC}/1.44V_{\tau F}}\right] \tag{2.104}$$

and τ_F is the ideal forward transit time.

One has to notice that $C_{\tau FF}$ is actually the modified version of the C_{DE} expression when the effects, that were described before, take place.

Finally, the distributed phenomena occurring in the base region are discussed. The phenomenon is characterized by the fact that, when the phase shift in the forward transverse current is measured from the actual devices, it tends to surpass the phase shift predicted by the lumped set of poles and zeros within the model [1]. Therefore, it is necessary to introduce an additional phase delay in the model as eq.(2.105) [1]:

$$I_{FX} = I_{CC}(\text{with the excess phase}) = I_{CC}\phi(s) \tag{2.105}$$

This effect is modelled by a second order Bessel function in order to avoid small step time in the transient analysis. Such function, in the frequency domain, is given by [1]

$$\phi(s) = \frac{3\omega_0}{s^2 + 2\omega_0 s + 3\omega_0^2} \tag{2.106}$$

in the time domain this function resembles a time-domain delay for a Gaussian curve, which is similar to the physical phenomenon exhibited by the transistor action. The phase shift is given by the function [1]

$$\theta = \arctan\frac{3\omega_0\omega}{3\omega_0^2 - \omega^2} \tag{2.107}$$

For $\omega < \omega_0$, the phase is written as the binomial expansion of the arctangent as $\theta = \omega/\omega_0$. Assuming $P_{\tau F}$ is the phase delay at maximum bandwidth $\omega = 1/\tau_F$, it can now be written as [1]

$$\omega_0 = \frac{1}{P_{\tau F}\tau_F} \tag{2.108}$$

This phase shift is implemented by adding the appropriate linear phase to the forward transverse term of the collector current I_{CC} [1]. By means of the inverse Laplace transform of $\phi(s)$, one can write the following differential equation [1]:

$$\frac{d^2 I_{FX}}{dt^2} + 3\omega_0 \frac{dI_{FX}}{dt} + 3\omega_0^2 I_{FX} = 3\omega_0^2 I_{CC} \tag{2.109}$$

This is equation is then implemented by performing a numerical integration algorithm.

Concerning the small-signal model the equations will be introduced when there will be the need. However, such equations may be consulted in [1].

2.3.1 Temperature dependence of BJT model parameters.

The temperature appears explicitly in the exponential term of the BJT model equations. In addition, the BJT parameters needs to be modified so to reflect changes in the temperature. They are I_S, the saturation current; C_2(or I_{SE}), the base-emitter leakage saturation current; C_4(or I_{SC}), the base-collector leakage saturation current; V_{JE} the base-emitter built-in potential; V_{JC} the base-collector built-in potential; β_F the forward current gain; β_R the reverse current gain; C_{JC}, the zero-bias base-collector depletion capacitance; V_{JE} the zero-bias base-emitter depletion capacitance; and FC the coefficient for forward-bias depletion capacitance formula.

The temperature dependence of I_S is given by the following equation [1]:

$$I_S(T_2) = I_S(T_1)\left(\frac{T_2}{T_1}\right)^{X_{TI}} \exp\left[-\frac{qE_g(T_1)}{kT_2}\left(1-\frac{T_2}{T_1}\right)\right] \tag{2.110}$$

where the new two parameters are X_{TI} which is the saturation current temperature exponent and E_g is the energy gap. One should notice that the energy gap also vary with the temperature and its variation with the temperature is described by the following equation [1], [12]:

$$E_g(T) = E_{g0} - \frac{\alpha T^2}{\beta + T} \tag{2.111}$$

where E_{g0}, α and β are determined empirically, and the values depend on the material used to build the BJT.

The effect of the temperature on the built-in potential is given by [1]:

$$\begin{aligned} V_{JE}(T_2) &= \frac{T_2}{T_1}V_{JE}(T_1) - 2\frac{kT_2}{q}\ln\left(\frac{T_2}{T_1}\right)^{1.5} - \left[\frac{T_2}{T_1}E_g(T_1) - E_g(T_2)\right] \\ V_{JC}(T_2) &= \frac{T_2}{T_1}V_{JC}(T_1) - 2\frac{kT_2}{q}\ln\left(\frac{T_2}{T_1}\right)^{1.5} - \left[\frac{T_2}{T_1}E_g(T_1) - E_g(T_2)\right] \end{aligned} \tag{2.112}$$

Regarding the temperature dependence of β_F and β_R their expressions are given by [1]:

$$\begin{aligned} \beta_F(T_2) &= \beta_F(T_1)\left(\frac{T_2}{T_1}\right)^{X_{T\beta}} \\ \beta_R(T_2) &= \beta(T_1)\left(\frac{T_2}{T_1}\right)^{X_{T\beta}} \end{aligned} \tag{2.113}$$

And through the parameter I_{SE} and I_{SC} the temperature dependence of C_2 and C_4, respectively, are found too and their expressions are [1]:

$$I_{SE}(T_2) = I_{SE}(T_1)\left(\frac{T_2}{T_1}\right)^{-X_{T\beta}}\left[\frac{I_S(T_2)}{I_S(T_1)}\right]^{1/n_{EL}}$$
$$I_{SC}(T_2) = I_{SC}(T_1)\left(\frac{T_2}{T_1}\right)^{-X_{T\beta}}\left[\frac{I_S(T_2)}{I_S(T_1)}\right]^{1/n_{CL}} \quad (2.114)$$

The temperature dependence of C_{JE} and C_{JC} is determined by [1]:

$$C_{JE}(T_2) = C_{JE}(T_1)\left\{1 + m_E\left[400\times10^{-6}(T_2 - T_1) - \frac{V_{JE}(T_2) - V_{JE}(T_1)}{V_{JE}(T_1)}\right]\right\}$$
$$C_{JC}(T_2) = C_{JC}(T_1)\left\{1 + m_C\left[400\times10^{-6}(T_2 - T_1) - \frac{V_{JC}(T_2) - V_{JC}(T_1)}{V_{JC}(T_1)}\right]\right\} \quad (2.115)$$

The temperature dependence of the coefficient for forward-bias depletion capacitance formula is determined by [1]:

$$FCPE(T_2) = FC\times V_{JE} = FCPE(T_1)\frac{V_{JE}(T_2)}{V_{JE}(T_1)}$$
$$F_1(T_2) = F_1(T_1)\frac{V_{JE}(T_2)}{V_{JE}(T_1)} \quad (2.116)$$

$$FCPC(T_2) = FC\times V_{JC} = FCPC(T_1)\frac{V_{JC}(T_2)}{V_{JC}(T_1)}$$
$$F_1(T_2) = F_1(T_1)\frac{V_{JC}(T_2)}{V_{JC}(T_1)} \quad (2.117)$$

3. Customized implementation of the Gummel-Poon Model in ADS

3.1. Derivation and implementation of the model

The equations derived thus far are intended to be utilized in order to implement the Gummel-Poon model on ADS Keysight. To this end, as will be illustrated below, the SDD component will be used, with the number of ports being adjusted during the model development process.

3.1.1 DC Model Derivation.

Before diving into the detail of the implementation of the Gummel-Poon model, a short description of the SDD component needs to be given [13].

The SDD component, i.e., Symbolic Defined Device, is a multi-port element which enables the user to define and implement linear e non-linear components alike by means of the behavioral equation characterizing the component under consideration.

Each of the port, for example port k is characterized by means of the port's current $_i_k$ and the port's voltage $_v_k$. There two ways to define the relation between the current and voltage at a given port, e.g. port k :

- Defining an implicit equation $f(_v_1, \dots, _v_k, \dots, _v_n, _i_1, \dots, _i_k, \dots, _i_m) = 0$
- Defining an explicit equation $i_k = f(_v_1, \dots, _v_k, \dots, _v_n)$

The implicit equation permits the user to define the port's current $_i_k$ as a variable to be inside the equation of another port's current $_i_n$, with the following syntax

$$F[k, q] = f(_v_1, \dots, _v_k, \dots, _v_n, _i_1, \dots, _i_k, \dots, _i_m)$$

where k is the port's number, and q is the weighting, i.e., the order of the time derivatives applied to the specified function. However, it is also possible to define other weightings, different from the time derivative, by means of the weighting function $H[q]$, which acts as a sort of filter's transfer function.

To the contrary if the port's current $_i_k$ is defined by an explicit equation with the syntax

$$I[k, q] = f(_v_1, \dots, _v_k, \dots, _v_n)$$

where k and q retain the same meaning as the implicit form, the current can no longer be used as a variable in the equation defining port's current $_i_n$.

Now that the SDD component has been introduced, the implementation of the Gummel-Poon static model can be initiated. To accomplish this, an SDD with three ports is utilized, with each port being assigned the following functions:

- Port one is used to perform a dual function: the first is to serve as the nonlinear resistance $r_{BB'}$, whose expression is given in eq. (2.85) , and the second is to simultaneously function as the pin for the transistor's base.
- The second port will be used as the collector of the BJT.
- The third port will be used as the emitter of the BJT.

Fig. 15 illustrates how to connect the three ports to one another in order to obtain the pins for the base, emitter, and collector, as well as the inclusion of the parasitic resistances r_C and r_E.

Additionally, three extra resistances are shown, which are used to obtain the node voltages referenced to ground.

One needs to implement the non-linear resistance on port 1. This is done by defining an implicit equation $F[1,0]$ for the SSD and by defining as a variable on $r_{BB'}$ on ADS, the latter part requires the use of the z parameter defined in eq.(2.86) and the mathematical behavior of the function defining $r_{BB'}$ needs to be taken into account. Indeed, recalling both of the expressions the one for $r_{BB'}$ and the one for z it can be noticed that as I_{rB} increases, z tends to zero, resulting in an indeterminate form for the expression of $r_{BB'}$ impairing the DC convergence of the SDD. In order to solve this problem, the limit of the function defining $r_{BB'}$ has been computed, and its value is

$$\lim_{z\to 0} r_{BB'}(z) = r_B \tag{3.1}$$

Then the $r_{BB'}$ is implemented as the piecewise function defined as:

$$r_{BB'}(z)\big]_{z=z_0} = \begin{cases} r_B & -10^{-12} < z_0 < 10^{-12} \\ r_{BB'}(z_0) & \text{otherwise} \end{cases}$$

Since the DC convergence problem is solved, the following implicit equation for port 1 can be safely defined:

$$F[1,0] = _i_1 \cdot r_{BB'} - _v1 \tag{3.2}$$

where in general the variables $_i_n$ and $_v_n$ indicate the current and the voltage at port n.

The current of the collector pin has been defined with opposite sign with respect the one presented in eq.(2.87), this has to be done in order to have the current flowing in the minus pin of port 2.

Regarding the current of the emitter the same reasoning has been followed and the two current are defined as function of the V_{BE} and V_{BC} as follow:

- A diode function, which will be used to avoid repeating the expression of the form $I_S\left(e^{qV/nkT} - 1\right)$,is implemented; this function is called $\mathrm{diode}(V, I_S, n)$ having as first argument the voltage V, as second argument the current I_S and as third argument the factor n
- The functions ICT, ICC and IEC, which represent the currents I_{CC}, I_{EC} and I_{CT} respectively, are implemented as described by the expressions in eqs.(2.13)-(2.14). In these implementations, the saturation current I_S is replaced with the modified saturation current I_{SS} , as defined in eq. (2.62) , and (2.66) respectively. The corresponding expressions are provided in the equations below:

$$ICC(V_{BE}) = \text{diode}(V_{BE}, I_{SS}, n_F)$$

$$IEC(V_{BC}) = \text{diode}(V_{BC}, I_{SS}, n_R) \tag{3.3}$$

$$ICT(V_{BE}, V_{BC}) = \frac{ICC(V_{BE}) - IEC(V_{BC})}{q_b}$$

- The I_E and I_C are given by:

$$\begin{aligned} I_C(V_{BE}, V_{BC}) &= -\text{ICT}(V_{BE}, V_{BC}) + \text{diode}(V_{BC}, I_{SC}, n_{CL}) + \frac{\text{IEC}(V_{BC})}{\beta_\text{R}} \\ I_E(V_{BE}, V_{BC}) &= \frac{\text{ICC}(V_{BE})}{\beta_F} + \text{diode}(V_{BE}, I_{SE}, n_{EL}) + \text{ICT}(V_{BE}, V_{BC}) \end{aligned} \tag{3.4}$$

Now it is all ready to use them inside the SDD so to define the currents that have to flow in ports two and three.

At this point of the implementation the number of fingers and the emitter width has been taken into account, which leads to the implicit equations for port two and three as shown below:

$$\begin{aligned} F[2,0] &= \left(N_{finger} \cdot Sizeumsq\right) \cdot I_C(_v_3, _v_2) - _i_2 \\ F[3,0] &= \left(N_{finger} \cdot Sizeumsq\right) \cdot I_E(_v_3, _v_2) - _i_3 \end{aligned} \tag{3.5}$$

Moreover, since the expression of $r_{BB'}$ depends on the value of the base current, from KLC applied to the node VB in Fig. 15 the following variable is defined:

$$IB = _i_2 + _i_3 \tag{3.6}$$

To prevent DC convergence issues, it is necessary to apply a condition to the base current (IB) and define the final variable, which will be used to compute $r_{BB'}$, as follow:

$$Ibb = \text{if}(IB < 1\text{e} - 12) \text{ then } 1\text{e} - 12 \text{ else } IB \text{ endif} \tag{3.7}$$

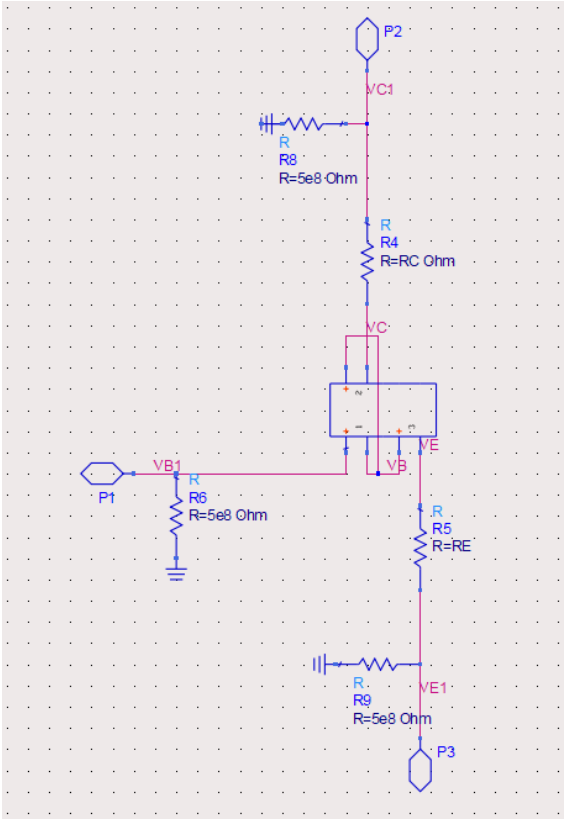

Fig. 15 The DC Model schematics in ADS

3.1.2 DC Model Testing.

Once all the required equations and connections have been implemented in the ADS schematic, the necessity to use an additional idealized model based on the injection version of the Ebers-Moll model emerges. This model will henceforth be referred to as the "EM Model" for simplicity. The purpose of employing this model is to ensure that the results obtained under the same conditions are consistent.

The process begins by creating symbols for the two BJTs and connecting them to their respective models. Once this is completed, the DC simulation can be properly configured. The DC simulation is set using the DC Curve Tracer component provided by ADS, allowing the

specification of the base current range and the collector-emitter voltage range. The parameters for the EM model are set as show in Table.1

Parameter	Value
n_F	1
n_R	1
β_F	100
β_R	2
I_{ES}	$4.9995 \cdot 10^{-15}\ A$
I_{CS}	$7.425 \cdot 10^{-15}\ A$

Table.1- EM Parameters

The parameters for the Gummel-Poon model are set so to reduce the model to the Ebers-Moll model as show in the table

In order to obtain the correct value for the parameter I_{SS},n_F and n_R, the curve I_C versus V_{BE} for $V_{BC} = 0$ for the EM Model has been fitted to the I_C when $V_{BC} = 0$, and considering all the other parameters fixed to their ideal value. The simulation schematic is set as it is shown in Fig. 16

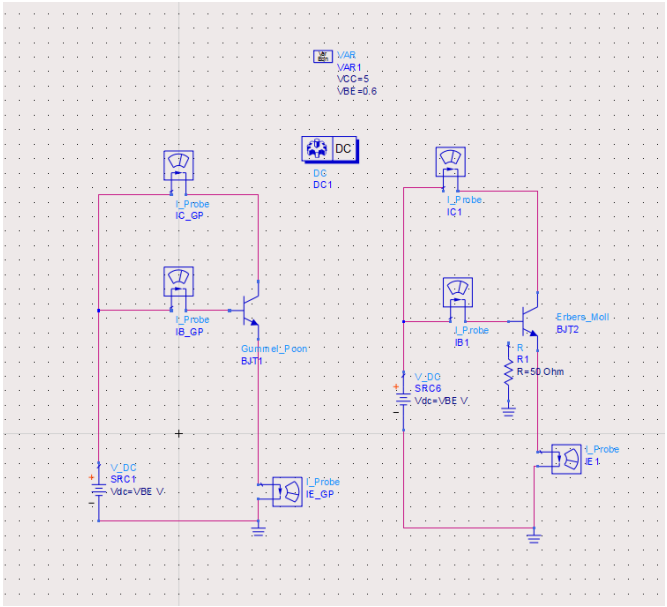

Fig. 16.Simulation Schematic used for the fitting

Running the simulation, the matching for I_C vs V_{BE} is obtained by setting I_{SS} and all of the other parameters as shown in Table.2, and the plot resulting from the simulation is shown in Fig. 17.

Parameter	Value
n_F	1
n_R	1
n_{EL}	1.5
n_{CL}	2
β_F	100
β_R	2
I_{SS}	$1.2375 \cdot 10^{-15}\ A$
I_{SE}	$0\ A$
I_{SC}	$0\ A$
V_A, V_B	$1 \cdot 10^{18}\ V$
I_{rB}	$1 \cdot 10^{18}$
I_{KF}, I_{KR}	$1 \cdot 10^{18}$

Table.2 – Gummel-Poon Parameters

The blue points are indicating the value obtained from the Ebers-Moll model meanwhile the red curved is indicating the Gummel-Poon model results, confirming the matching.

Now, the simulation is set in order to compare the curves I_C versus V_{CE}.

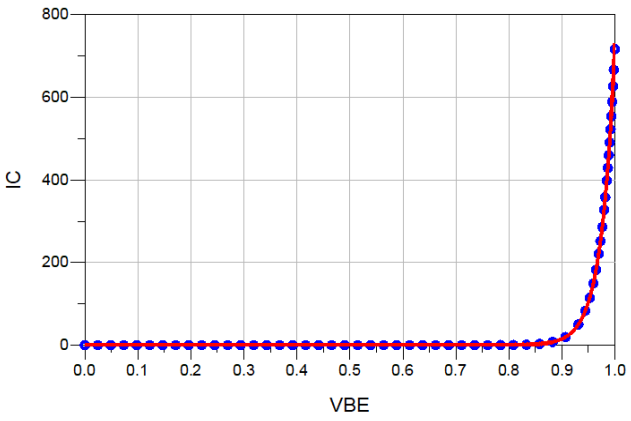

Fig. 17 $I_C(in\ Ampereé)$ versus $V_{BE}(in\ Volt)$ curve.

As mentioned before, the BJT Curve Tracer of ADS is used so to perform the comparison, as shown in figure below.

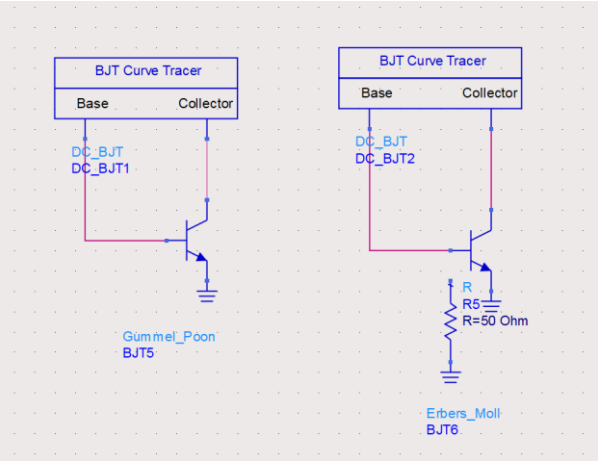

Fig. 18- Schematic for DC Testing of I_C vs. V_{CE}

The results of the simulation are shown in Fig. 19. From it, one notices that the results obtained by the Ebers-Moll for fixed values of I_B(blue circles), and the results obtained from the Gummel-Poon for the same fixed values of I_B(red curves) are perfectly overlapping.

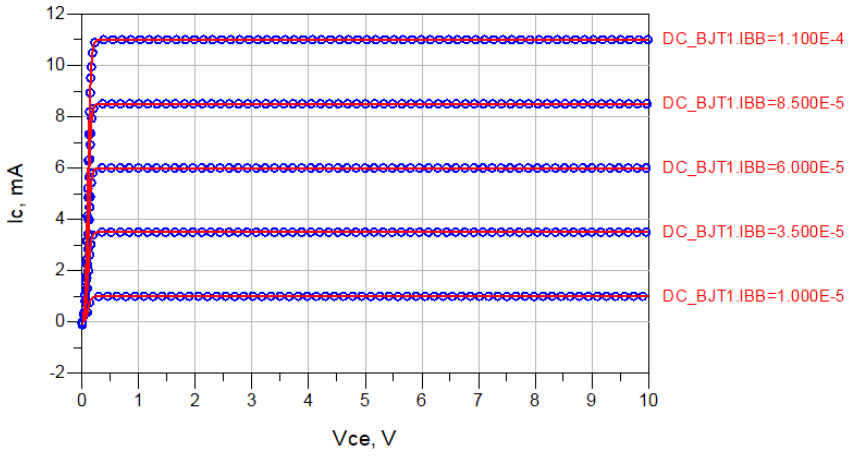

Fig. 19 I_C vs V_{CE} plot.

3.1.3 AC Model Derivation.

The parasitic capacitances C_{BE} and C_{BC} are now included into the model so to take in account the frequency behavior of the BJT too. In order to do so the schematic of the Gummel-Poon model is modified in the following way:

One recalls that the base-emitter C_{BE} and C_{BC} collector-base capacitances are given by the sum of two contributions, the first contribution is given by the diffusion capacitances C_D and the second one is given by the junction capacitances C_J.

Particularly, the junction capacitances are given by means of the following equations

$$C_{JC} = \begin{cases} C_{JC0}\left(1 - \dfrac{V_{BC}}{V_{JC}}\right)^{-m_C} & \text{for } V_{BC} < FC \times V_{JC} \\ \dfrac{C_{JC0}}{F_2}\left(F_3 + \dfrac{m_C V_{BC}}{V_{JC}}\right) & \text{for } V_{BC} \geq FC \times V_{JC} \end{cases} \tag{3.8}$$

$$C_{JE} = \begin{cases} C_{JE0}\left(1 - \dfrac{V_{BE}}{V_{JE}}\right)^{-m_E} & \text{for } V_{BE} < FC \times V_{JE} \\ \dfrac{C_{JE0}}{F_2}\left(F_3 + \dfrac{m_E V_{BE}}{V_{JE}}\right) & \text{for } V_{BE} \geq FC \times V_{JE} \end{cases} \tag{3.9}$$

whereas the diffusion capacitance for the collector-base is given by the equation

$$C_{DC} = \tau_R \frac{dI_{EC}}{dV_{BC}} \tag{3.10}$$

and by carrying out the derivative with respect to the V_{BC}, it gives

$$C_{DC} = \tau_R \frac{I_{SS}}{n_R V_T} e^{V_{BC}/n_R V_T} \tag{3.11}$$

In order to write down the equation describing the diffusion capacitance of the emitter-base region, eq.(2.103) is needed, which is provided below for convenience

$$C_{DE} = \frac{\partial}{\partial V_{BE}}\left(\tau_{FF} \frac{I_{CC}}{q_b}\right) \tag{3.12}$$

Indeed, this expression for C_{DE} is required once the effect of the τ_F modulation and in the high-current injection are considered.

The performing of derivative leads to

$$\begin{aligned} C_{DE} = \frac{2\tau_F}{q_b}\frac{(ATF-1)I_{\tau F}}{(I_{CC}+I_{\tau F})}\frac{I_{SS}}{n_F V_T}e^{V_{BE}/n_F V_T} + \frac{ATF\cdot\tau_F}{q_b}\frac{I_{SS}}{n_F V_T}e^{V_{BE}/n_F V_T} + \\ -ATF\cdot\tau_F I_{CC}\frac{q_1}{q_b}\left[\frac{1}{V_{AR}} + \frac{1}{q_b}\frac{1}{\sqrt{(1+4q_2)^3}}\frac{1}{n_F V_T}\frac{I_{SS}}{I_{KF}}e^{V_{BE}/n_F V_T}\right] \end{aligned} \tag{3.13}$$

Since one wants to compare the behavior of the Gummel-Poon against the one provided by the Ebers-Moll; the appropriate simulation conditions have to be taken into account, in particular, the Ebers-Moll under consideration is an ideal one which does not include the Early voltage effect.

This fact imply that one should let the V_{AR} and V_{AF} tend to infinity, moreover also the knee currents I_{KF} and I_{KR} should tend to infinity, which leads one to have q_1, q_2 and q_b of the order of the unit. In addition to this, the term between square bracket in the third member of eq.(3.13) goes to zero under the specified conditions.

Regarding the first member of the above expression, since the ideal case is assumed, the τ_F modulation effect vanishes leading to set $X_{\tau F} = 0$ and $I_{\tau F} \to +\infty$ resulting in $ATF \approx 1$. This implies that the first member vanishes too.

Finally, one is left with the following expression for C_{DE}

$$C_{DE} = \tau_F \frac{I_{SS}}{n_F V_T} e^{V_{BE}/n_F V_T} \tag{3.14}$$

which is exactly the expression for the emitter diffusion capacitance for the Ebers-Moll.

These capacitances must be incorporated into the ADS model. To achieve this, three additional ports are required, as depicted in Fig.20. These ports are used to compute the time derivative of V_{BE} and V_{BC} , after which the resulting values are multiplied by the corresponding capacitance values. Specifically, the following explicit equations are used to define the behavior of ports four, five, and six:

$$\begin{aligned} I[4,1] &= _v_2 \\ I[5,1] &= _v_3 \\ I[6,1] &= _v_1 + _v_2 \end{aligned} \tag{3.15}$$

Since the time-derivative of voltage is the quantity of interest, a 1 Ω resistance at each of the port is used as conversion factor.

Finally, these contributions are added in accordance with the following equations:

$$\begin{aligned} F[2,0] &= \left(N_{finger} \cdot Sizeumsq\right) \cdot \left[I_C(_v_3, _v_2) - \left(C_{JC} + C_{DC}\right) \cdot _v_4 - C_{JX} \cdot _v_6\right] - _i_2 \\ F[3,0] &= \left(N_{finger} \cdot Sizeumsq\right) \cdot \left[I_E(_v_3, _v_2) - \left(C_{JE} + C_{DE}\right) \cdot _v_5\right] - _i_3 \end{aligned} \tag{3.16}$$

In our ADS model the voltages V_{BE} and V_{BC} were, respectively, $_v_3$ and $_v_2$, whereas V_{BX} ,on whose value will depend the value of C_{JX},was $_v_1 + _v_2$. Moreover, one needed to account for the area of the emitter and the number of fingers, therefore all of the current across the capacitances have been multiplied by the factor $N_{finger} \cdot Sizeumsq$.

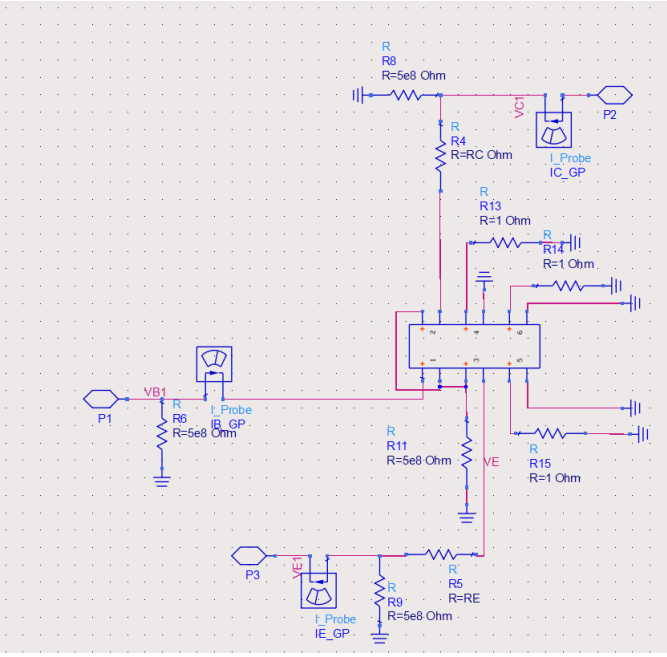

Fig.20 ADS Schematic with the added parasitic capacitances.

The schematic of the model including the parasitic capacitances is shown in Fig.20. The new parameters need to be set properly to ensure consistency between the AC simulation results of the GP and EM models. This will be addressed in the following section.

3.1.4 AC Model Testing.

In the previous paragraph it was showed how to implement the AC Model starting from the mathematical equation, now one aims to test the model against the Ebers-Moll model that was also used for the DC testing.

One begins with listing all of the necessary parameters that will be needed to obtain some agreement between the results from the comparison of both models. Such parameter and their tuned values are listed in Table.3; moreover, for simplicity, in this table the DC parameters will not be included, which are assumed to be the ones indicated when the DC testing was discussed, but the parameters' value used for the Ebers-Moll model AC behavior will be included.

One should notice that the parameters $X_{CJC}, X_{\tau F}, V_{\tau F}$ and $I_{\tau F}$ are not defined in the Ebers-Moll model, therefore, the same value, at which the Gummel-Poon model behaves as the Ebers-Moll, needs to be set.

Since the Ebers-Moll model used for the comparison did not implement any diffusion capacitances, this fact is interpreted as having ideal transit times, i.e. $\tau_F = 0$ and $\tau_R = 0$.

In order to fine tune the junction capacitances, one needs to measure these capacitances on the Ebers-Moll model with respect to the voltages across them; in particular, this means that the plots C_{JE} vs. V_{BE} and C_{JC} vs. V_{BC} are needed.

Parameter	Ebers-Moll Value	Gummel-Poon Value
C_{JC0}	$10^{-21}\ F$	$2.5 \cdot 10^{-22}\ F$
C_{JE0}	$10^{-21}\ F$	$2.5 \cdot 10^{-22}\ F$
C_{CE}	$10^{-25} F$	$10^{-25} F$
V_{JE}	$0.7\ V$	$0.7\ V$
m_E	0.5	0.5
V_{JC}	$0.7\ V$	$0.7\ V$
m_C	0.5	0.5
FC	0.7	0.7
X_{CJC}	1	1
τ_F	$0\ s$	$0\ s$
τ_R	$0\ s$	$0\ s$
$X_{\tau F}$	0	0
$V_{\tau F}$	$10^{18}\ V$	$10^{18}\ V$
$I_{\tau F}$	$10^{18}\ V$	$10^{18}\ V$

Table.3 Tuned Value for Gummel-Poon and Ebers-Moll

To this end the following relations, linking the value of junction capacitances with admittance parameters, are used; in particular, it is easy to show that [3]:

$$C_{BE} = \frac{1}{\omega} Im\{Y_{11} + Y_{12}\}$$
$$C_{BC} = -\frac{1}{\omega} Im\{Y_{12}\} \qquad (3.17)$$

Under the operative conditions said before, it is clear that C_{BC} will be equal to C_{JC} and C_{BE} will be equal to C_{JE}. The S-parameter simulation tool is set to compute the Y parameters at a working frequency of $1\ MHz$; then the Sweep Parameter tool is used in order to vary V_{BE} or V_{BC} one at the time.

A common-emitter configuration is set up, with the end goal in mind of measuring C_{JE} the collector is biased with a voltage $V_{CC} = 5V$, and the base with a voltage $V_{BB} = 0.7$ as initial value. Then since the emitter is kept at the ground, we can vary V_{BE} by varying V_{BB} in the range 0 to 0.49 V. Regarding C_{JC}, one keeps the base biased at $0.7V$, and lets V_{CC} varying in the range 0.21 to 0.7 V.

Once the simulation has finished, by means of measurement equations, the relation given in eq.(3.17) is implemented. From the plot, one finds out that:

$$C_{JC0} = C_{JC}(V_{BC} = 0) = 2.5 \cdot 10^{-22}\ F$$
$$C_{JE0} = C_{JE}(V_{BE} = 0) = 2.5 \cdot 10^{-22}\ F \qquad (3.18)$$

These values are chosen for the Gummel-Poon model, and the same procedure is repeated so to compare the plots, and as result of the comparison one finds that the two plots perfectly match.

In the following figures the schematics for the simulation and their results are shown:

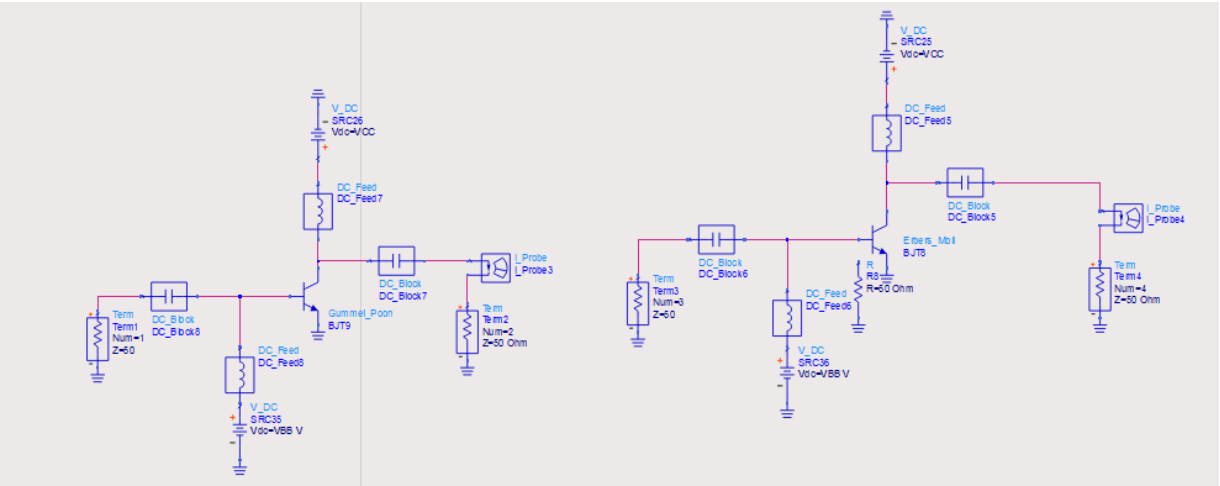

Fig.21 Setup for the parasitic capacitances' measurement

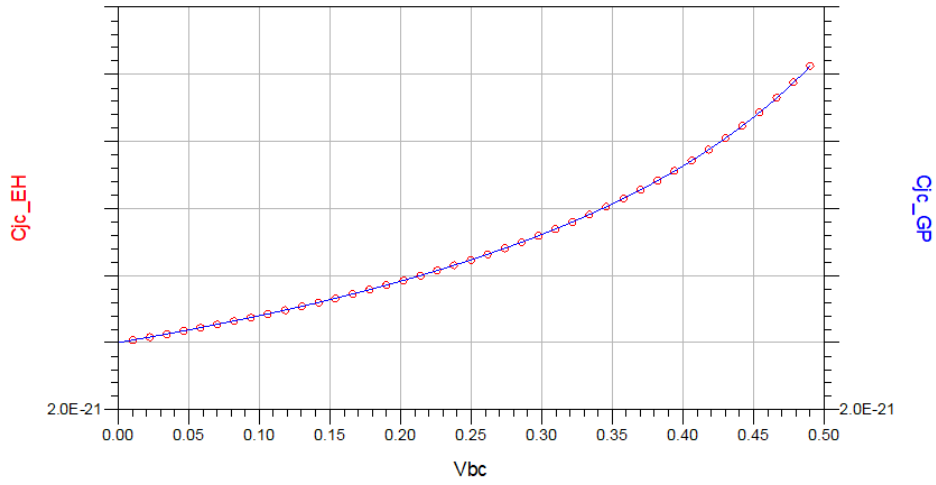

Fig.22 C_{JC} vs V_{BC}

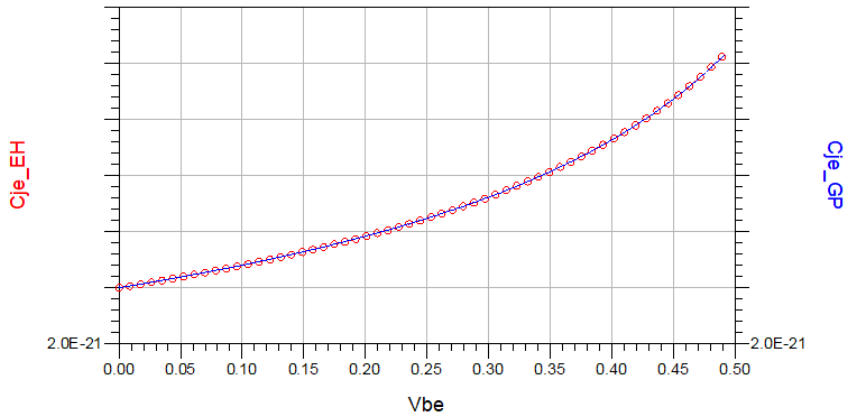

Fig.23 C_{JE} vs V_{BE}

In both Fig.22 and Fig.23, the red circles are indicating the results from the Ebers-Moll model, meanwhile the blue curve is indicating the results from the Gummel-Poon model.

One can, now, proceed to compare the results for the both model of the S-Parameters and the small-signal AC response. Using the same configuration as in Fig.21,where the DC Voltage generator is substituted with a DC Current one, the bias point for both model is set at $V_{CC} = 5\ V$ and, with a base current $I_B = 500\ \mu A$, a range of frequency that goes from 0 to 5 GHz, and the values of capacitance are changed with respect to Table.3 so to better show the behavior of the S parameter as the frequency varies.

$$\text{GP Model} \begin{cases} C_{JE0} = 100\ fF \\ C_{JC0} = 0.25\ fF \end{cases} \qquad \text{EM Model} \begin{cases} C_{JE0} = 400\ fF \\ C_{JC0} = 1\ fF \end{cases}$$

The S-parameters are the first to be tested; for the S_{22} of both models to agree, the Early Voltage of the Gummel-Poon model needs to be fine-tuned too; since the S_{21}, which is linked to the gain of the BJT and therefore linked to the transconductance g_m , are already matched. In particular we need to change its value indicated in Table.2 with the following, values

$$\begin{aligned} V_A &\approx 5 \cdot 10^6\ V \\ V_B &\approx 5 \cdot 10^6 V \end{aligned} \tag{3.19}$$

The results for the S-Parameter simulation are show in figure below

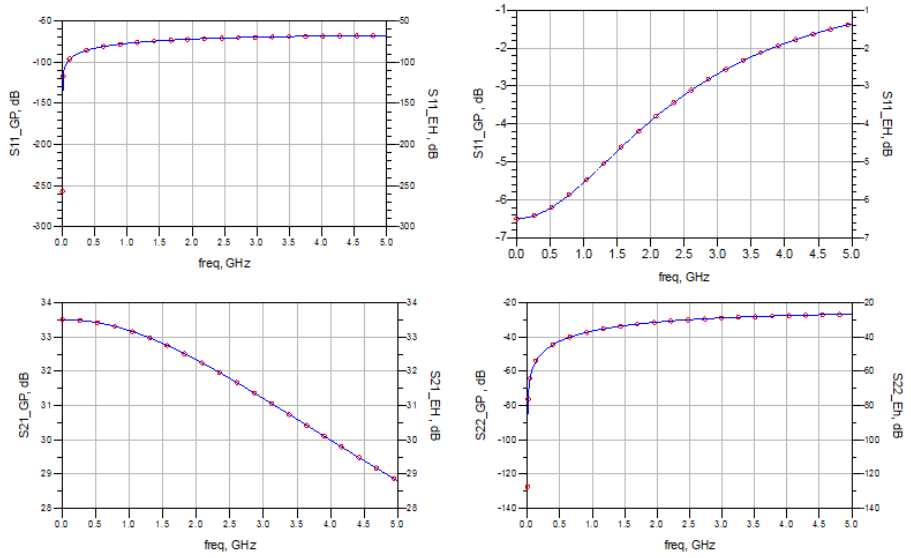

Fig.24 S-Parameters in dB vs. frequency

where, as usual, the red circles are showing the result from the Ebers-Moll Model, whereas the solid blue line is showing the result from the Gummel-Poon model; as expected the results from both models are in agreement.

The AC response in frequency of both model is now considered; the same configuration and bias point have been chosen, as we just used for the S-parameters, whereas the junction capacitances are set according to Table.3. One applies a one tone generator with an amplitude of $10\ mV$ while letting the frequency varying in the range 0 to $5\ GHz$; Finally, the results are plotted as modulus and phase in figure below.

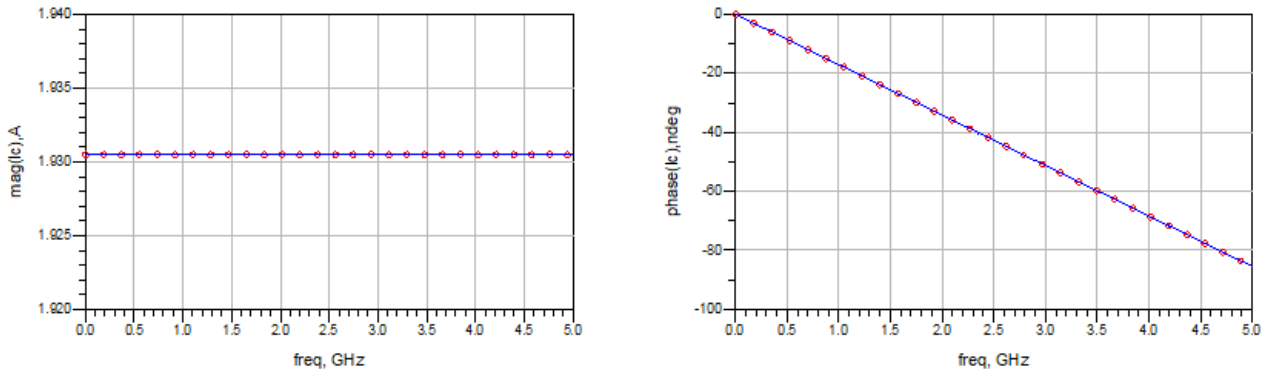

Fig.25 AC response, $|I_C|$ and $\measuredangle I_C$ vs frequency.

where the same convention as before is used in the plot in order to identify the results from both models, which are clearly in agreement.

3.1.5 Thermal Model Derivation.

In this subparagraph, the thermal effects will be now implemented.

This is done by implementing the formulas given by equations (2.110) to (2.117); therefore, one needs to implements a port to compute the temperature's variation and a port to compute the dissipated power. Indeed, the junction temperature of the device is depended on the dissipated power through the thermal resistance and their relationship is given by [14]

$$T_j - T_a = P_{diss} \cdot R_{TH} \tag{3.20}$$

where T_j and T_a are indicating the junction temperature and the ambient temperature respectively. This relation also allows to draw a parallel between the temperature and the dissipated power with the voltage and the current in the ohm law; and this fact will be used later on to model the thermal behavior, where the temperature will be treated as a voltage, the dissipated power as a current and the thermal resistance as an electrical resistance.

One needs to evaluate the dissipated power, in particular the average dissipated power, which is dissipated by the device. As it is known, in a BJT the dissipated power is given by [14]

$$P_{diss} = V_{CE} \cdot I_C + V_{BE} \cdot I_B \tag{3.21}$$

recalling that:

$$V_{CE} = V_{BE} - V_{BC} \tag{3.22}$$

then, one gets:

$$P_{diss} = V_{BE} \cdot I_E - V_{BC} \cdot I_C \tag{3.23}$$

If one recalls that when the DC part was implemented, I_C required a negative sign, due to the fact that $_i_2$ was entering through the negative pin of the port, the final expression is:

$$P_{diss} = _v_3 \cdot _i_3 + _v_2 \cdot _i_2 \tag{3.24}$$

The eq.(3.24) is however instantaneous dissipated power which can be converted into the average dissipated power by multiplying it for a suitable weighting function.

The required weighting function is characterized by a low-pass filter, as the thermal behavior can be approximated in this manner, at least as a first-order model. Consequently, it will assume the following form:

$$H(\omega) = \frac{H_0}{1 + j\omega\tau} \tag{3.25}$$

where H_0 is a suitable constant to be fitted, and τ is the time constant, linked to the thermal capacitance and the thermal resistance, the thermal process [14]. Considering that order of magnitude of τ is typically much larger than the period associated to the microwave frequency the only significant quantity left in eq.(3.25) is H_0.

At last, one is now able to write the final expression for the dissipate power as

$$P_{diss} = \frac{H_0}{1 + j\omega\tau} \cdot (_v_3 \cdot _i_3 + _v_2 \cdot _i_2) \tag{3.26}$$

In Fig. 26 shows the schematic of the model after the two ports have been added; in particular port 7 is the port where the average dissipated power is computed. Indeed, eq.(3.26) can be implemented in ADS as follows:

As a first, the explicit equation on port 7 is defined by

$$I[7,5] = _v_3 \cdot _i_3 + _v_2 \cdot _i_2 \tag{3.27}$$

then, the weighting function associated with the weighting index 5 has to be defined, since only the indices 0 and 1 are defined by default, and such function is given by eq. (3.25). For implementing it into ADS as it is shown in below

$$H[5] = \frac{H_0}{1 + j \cdot \omega \cdot \tau} \tag{3.28}$$

The output from port 7 corresponds to a current, the magnitude of which, expressed in amperes, represents the dissipated power in watts. Therefore, to measure the dissipated power, a current probe, referred to as P_diss, is utilized, as depicted in Fig. 26. Furthermore, it is important to note the inclusion of an additional pin, which is designed to allow the attachment of an external thermal resistance, thereby placing it in parallel with the internal thermal resistance. Finally, the current probe named I_DeltaT is used to measure the difference between the junction temperature and ambient temperature.

Concerning port 8, it is used in order to compute the junction temperature of the device according to the following equation

$$I[8,0] = -_v_7 + T_a \tag{3.29}$$

where $_v_7$ is the voltage at port 7, which is representing the difference between the junction temperature and the ambient temperature.

Now, that the quantities necessary to compute the temperature have been implemented, one can also implement the variable corresponding to the eqs.(2.110),(2.111),(2.113),(2.114)

as it is show in the following. In this subparagraph, the thermal effects will be now implemented.

Eq. (2.111) is the expression which relates how the energy gap varies with the varying temperature, for convince the expression of the energy gap is now recalled

$$E_g(T) = E_{g0} - \frac{\alpha T^2}{T + \beta}$$

This expression is implemented on ADS by defining two constants a and b which will substitute α and β in Eq.(2.111) plus an additional constant Eg which will be the constant representing E_{g0}.

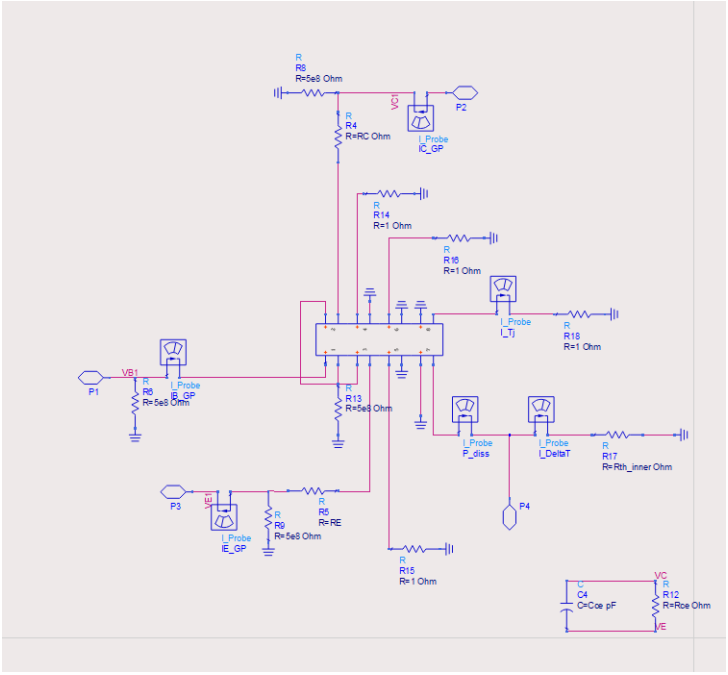

Fig. 26 ADS model with thermal effects included

The values for these three constants need to be chosen on the base of the material used for the construction of the actual device and, as an example for the testing of the model, such material will be assumed to be GaAs and therefore the forementioned constant will have the following values [12]:

$$\alpha = 5.8 \cdot 10^{-4}$$
$$\beta = 300$$
$$E_{g0} = 1.522\ eV$$

Regarding the temperature parameter T it has been implemented as a variable T_{jun} which represents the junction temperature indicated in eq.(3.29) but the ambient temperature is expressed in degree Kelvin, the expression of T_{jun} is given by

$$T_{jun} = -_v_7 + T_a \tag{3.30}$$

The eqs.(2.110),(2.113),(2.114) are modified accordingly as it follows:

Eq. (2.110) now reads

$$I_{SS}(T_{jun}) = I_{SS0}\left(\frac{T_{jun}}{T_a}\right)^{XTI} e^{-\frac{qE_g}{T_{jun}}\left(1-\frac{T_{jun}}{T_a}\right)}$$

Eqs. (2.113) become

$$\beta_F(T_{jun}) = \beta_{F0}\left(\frac{T_{jun}}{T_a}\right)^{X_{T\beta}}$$

$$\beta_R(T_{jun}) = \beta_{R0}\left(\frac{T_{jun}}{T_a}\right)^{X_{T\beta}}$$

Finally, eqs.(2.114) are rewritten as

$$I_{SE}(T_{jun}) = I_{SE0}\left(\frac{T_{jun}}{T_a}\right)^{-X_{T\beta}}\left[\frac{I_{SS}(T_{jun})}{I_{SS0}}\right]^{1/n_{EL}}$$

$$I_{SC}(T_{jun}) = I_{SC0}\left(\frac{T_{jun}}{T_a}\right)^{-X_{T\beta}}\left[\frac{I_{SS}(T_{jun})}{I_{SS0}}\right]^{1/n_{CL}}$$

where $I_{SS0}, I_{SE0}, I_{SC0}, \beta_{F0}$ and β_{R0} are denoting the respective quantity at room temperature.

Moreover, an additional parameter named thermal is added to each of the quantity. This parameter has the role to determine whether the thermal model is active or not, and this is done by implementing a simple if statement in ADS; in particular, when the parameter thermal value is equal to 1 then the modified equation listed above will be used, otherwise the constant value of each quantity at room temperature will be considered.

3.1.6. Thermal Model Testing.

In this subparagraph the model will be tested against the EM model as it was done previously; in particular, this aims to show the self-heating effect due to the increasing junction temperature in both model by the plot of I_C versus V_{CE}, each for model, and those are to be coinciding. The first task is to make a fitting for the parameter H_0 in eq. (3.28), whereas τ is given by means of the cutoff frequency of the thermal process, which is set to $1\ MHz$.

The fitting of H_0 is performed by setting the thermal parameter to one and then by plotting the dissipated power from both model while H_0 is varied until both the curves perfectly overlap. The schematic by which the formation operation is accomplished is shown Fig. 27. The I_B current is swept from $250\ \mu A$ to $750 \mu A$ whereas the V_{CE} voltage is swept from 0 to 10 Volt.

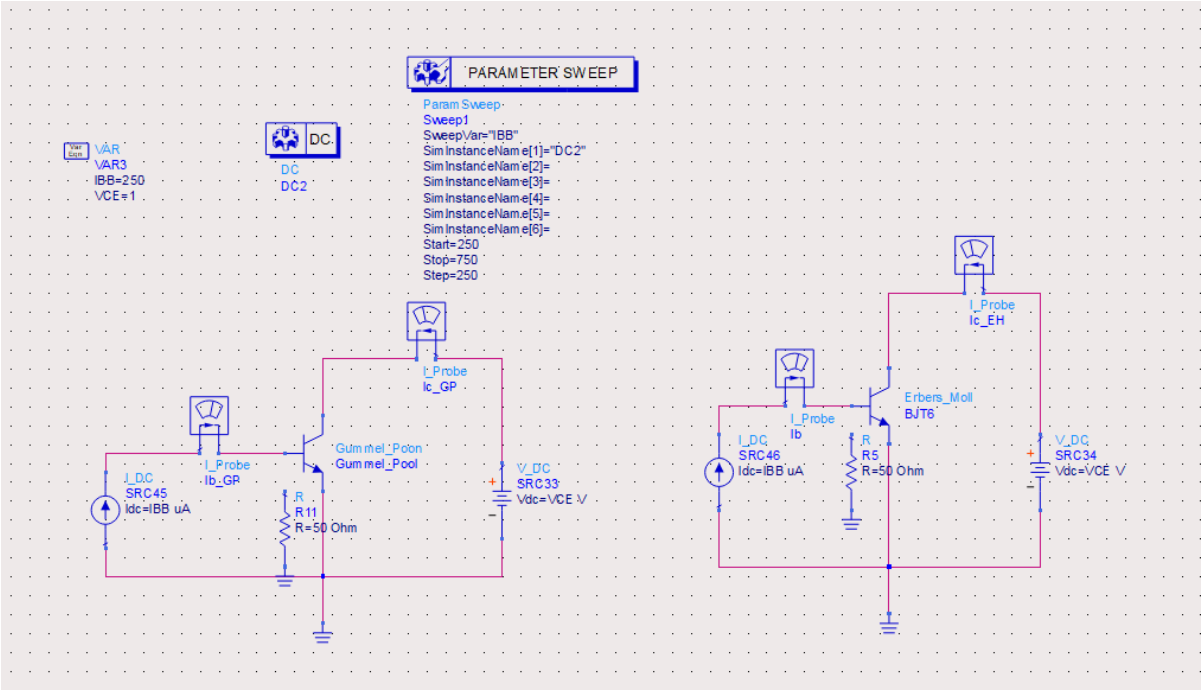

Fig. 27 Schematic use for the H_0 parameter tunning.

The curves finally coincide for coincide for a value of H_0 equals to

$$H_0 = 1$$

where the value has been truncated to the fourth decimal place. The result of the simulation is given in Fig.28; where, usual the red circles are indicating the results from the Ebers-Moll model

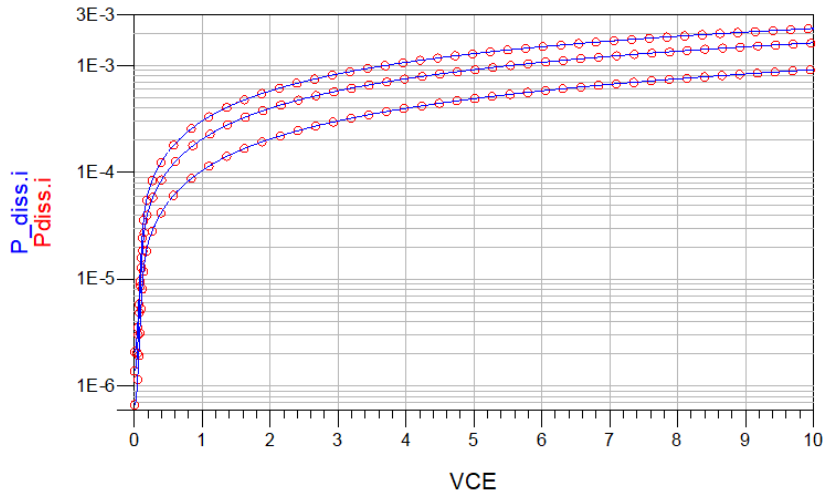

Fig.28 Dissipated power vs V_{CE} in semi-log scale.

whereas the blue solid line is showing the results for the Gummel-Poon model, and it is clearly seen the agreement between the two models.

As a further step, one needs to fit the internal thermal resistance of the Gummel-Poon model, since the external one will be assumed to be equal for both the model with a value $50°C/W$ so that also the temperature variation given by two model are in agreement. In this phase, the tune tool will be used once more, and the same schematic as the one in Fig.28 will be used; then by using the same procedure used for the tuning of the dissipated power, the value of the inner thermal resistance is equal to $R_{TH,inner} = 200$ °C/W. The results are shown by means of plot in Fig.29; where, by means of the usual legend for showing the results, one readily sees the agreement between the two models.

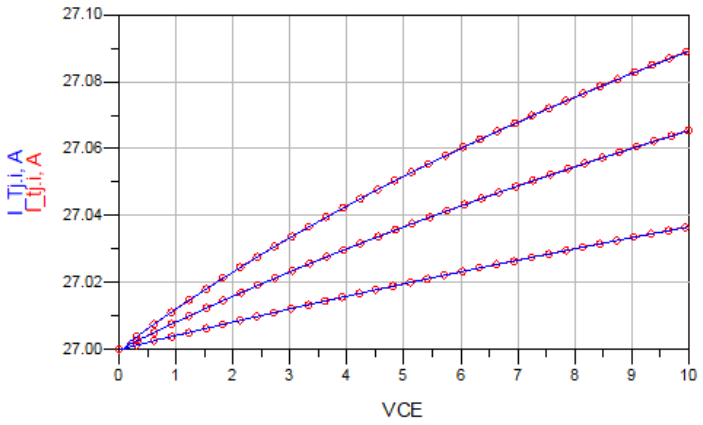

Fig.29 Junction Temperature Vs V_{CE}

The two parameters, that are remained to be determined in order to plot the I_C versus V_{CE} curves, are X_{TI} and $X_{T\beta}$. These are to be fitted so that forward current gain β_F and its relation with I_C and I_B is fulfilled. Therefore, with this goal in mind, the schematic shown in Fig.30

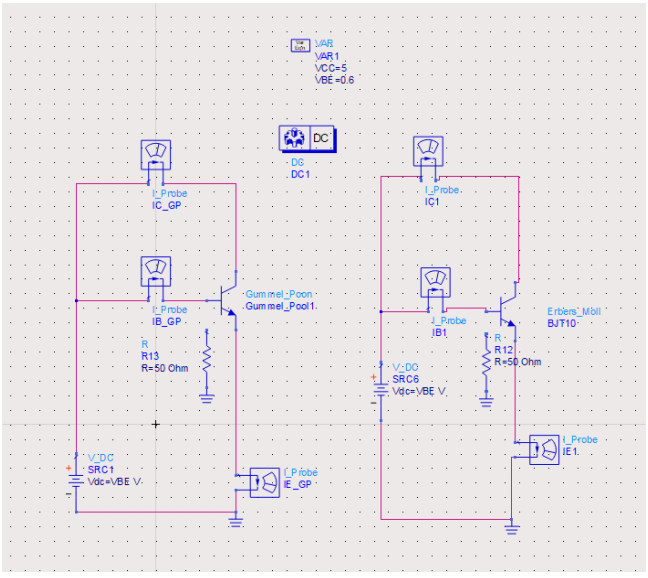

Fig.30 Schematic used for determining X_{TI} and $X_{T\beta}$

where the V_{BC} is set to zero so that the I_C vs V_{BE} and I_B vs V_{BE} curves can be plotted. Once obtained for both models, the curves corresponding to the Gummel-Poon model must be made

coincident with those provided by the Ebers-Moll model by varying X_{TI} and $X_{T\beta}$ with use of the tune tool.

Fig. 31 shows the results of the fitting performed using the schematic presented in Fig.30, with the observation that the results of the two models coincide when:

$$X_{TI} = -1210.84348$$

$$X_{T\beta} = -1199.763176$$

Finally, Fig.32 shows the characteristic curves of I_C versus V_{CE} as a function of the base current I_B, thereby illustrating the negative slope of the collector current, as the device's dissipated power increases leading to an increase in the junction temperature. In this case as well, it is observed that the results for both models are in perfect agreement.

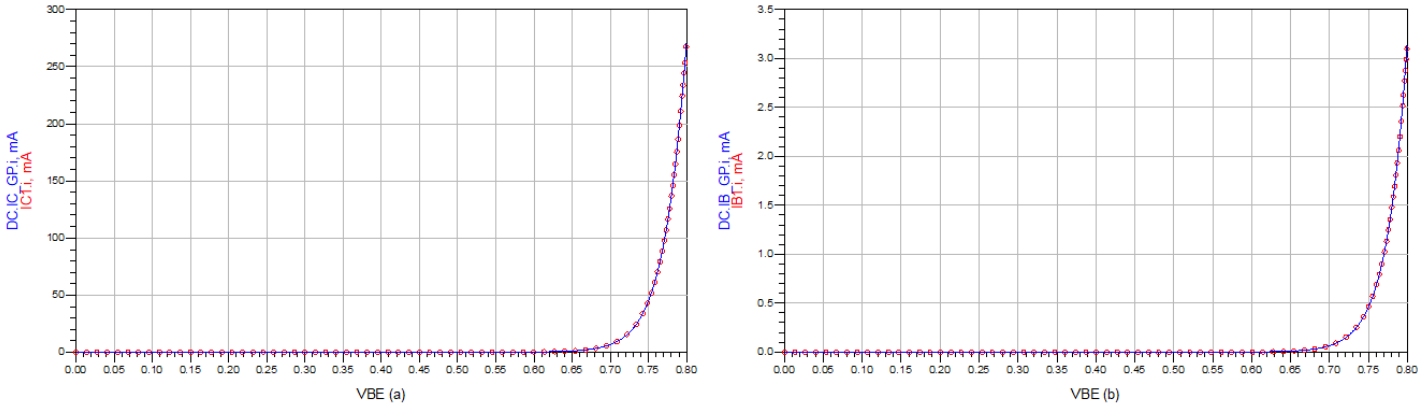

Fig. 31 The plots for I_C vs V_{BE} (a) and I_B vs V_{BE} (b)

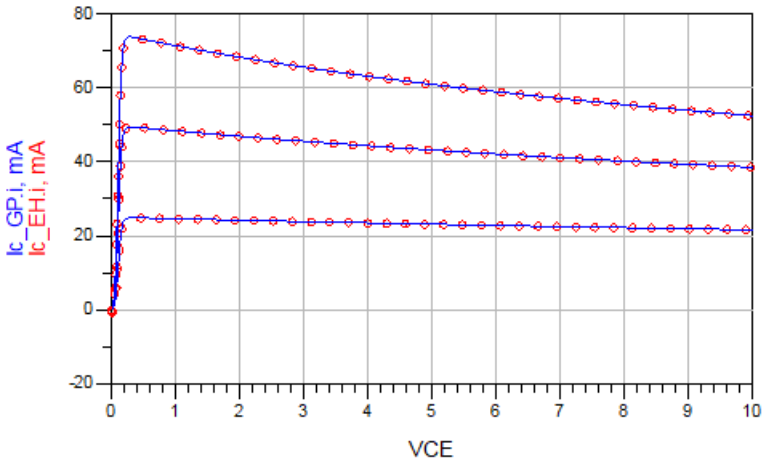

Fig.32 thermal self-heating effects on DC I_C vs V_{CE}

4.Implementation of class A and Class B amplifier

In this chapter, the implementation of class A and tuned class B amplifier is shown.

4.1. Design of the amplifiers and testing

In this paragraph, the design of the two amplifiers will be discussed; more precisely, in 4.1.1 The design of class A will be specifically presented when the self-consistent thermal model is active, meaning that the effects due to self-heating are taken into account. The results will be compared with those in which the self-heating effect is not considered. In 4.1.2 the design of a tuned class B will be presented, and a comparison will be made between the results obtained when thermal effects are included and when they are neglected.

the tuned version of the class B is designed and its results presented.

4.1.1. Class A amplifier and testing

The design of the class A amplifier begins, as it is easier, by neglecting the effects of self-heating, i.e. the thermal flag, implemented in 3.1.5, is set to 0. The bias point of the BJT is required to be chosen at the middle point of the voltage swing and for half of the maximum current [3]. For this example, the maximum value of V_{CE} is chosen to be equal to $10V$ and the maximum for the current I_C is chosen to be equal to $75\ mA$.

In normal active region the maximum collector current is achieved by imposing the maximum value of the base current, I_B, equals to $750\ \mu A$; therefore, a first approximation for the optimal resistance is obtained by assuming a $V_{CE,sat} = 0$ which leads to [3]

$$R_{opt} = \frac{V_{CE,max}}{I_{C,max}} = \frac{10V}{75\ mA} = 133\ \Omega$$

and the bias point is given by

$$V_Q = \frac{V_{CE,max}}{2} = 5V$$

$$I_Q = \frac{I_{C,max}}{2} = 37{,}5\ mA.$$

Fig.33 illustrates the schematic used to simulate the class A behavior when the self-heating is neglected.

Moreover, in order to obtain reasonable results, the following value of parasitic base resistance and junction capacitance have been chosen:

$$r_B = 10\ \text{Ohm}$$
$$C_{JC0} = 9 \cdot 10^{-14}\ \text{F}$$
$$C_{JE} = 3 \cdot 10^{-13}\ \text{F}$$

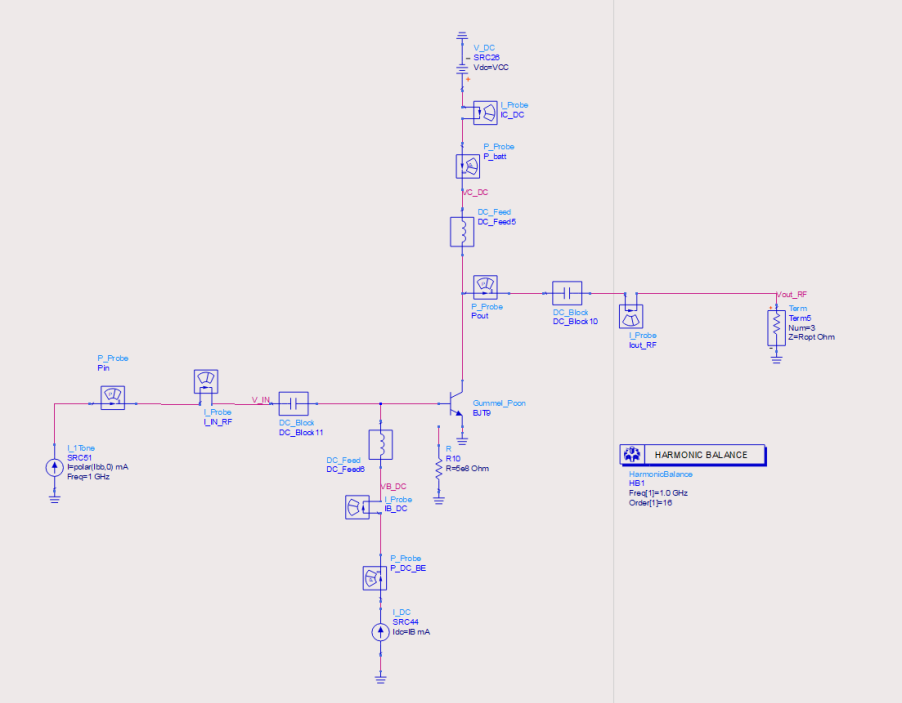

Fig.33 Harmonic Balance Schematics for the simulation of the class A when the self-heating effect is neglected

The results of the harmonic balance simulation are illustrated:

- **Verification of the quiescent point**

  The output characteristic of the BJT and the dynamic load line are plotted and as show in Fig.34 confirming the previous computations, as the quiescent point m_{13} is indeed at the intersection of the specified voltage and current.

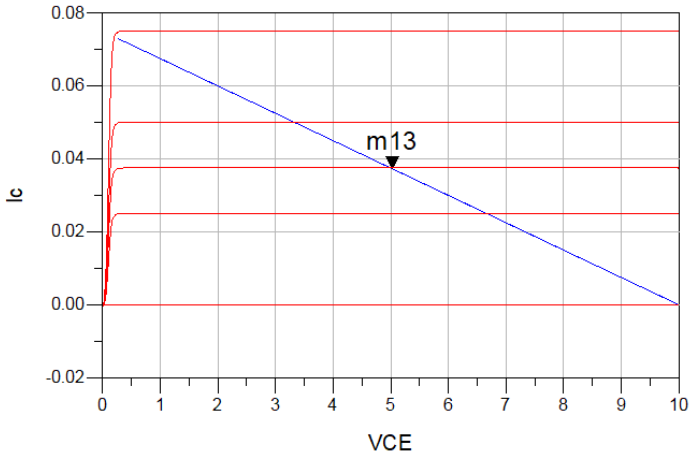

Fig.34 The load line in blue is interesting the output characteristic in red at the quiescent point m_{13}

- **Verification Pin-Pout characteristics and Gain**.

  The Pin-Pout characteristic and the Gain versus the Input power in logarithmic scale are shown in Fig.35 and Fig. 36 .

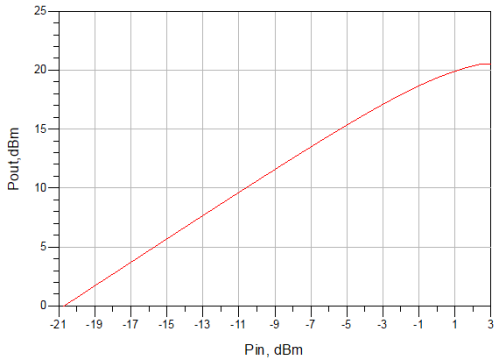

Fig.35 Pin-Pout Characteristic in logarithmic scale

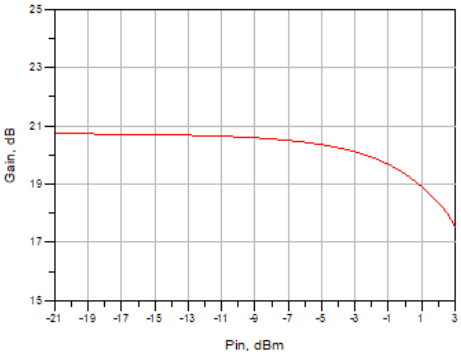

Fig. 36 Gain vs Pin in logarithmic scale

- **Verification of the dissipated power and junction temperature.**

  The self-heating effect is being neglected; this means that the model does not take into account the dissipated power implying that the temperature junction remains at room temperature, i.e. $27℃$. The dissipated power as a function of the input power will be shown in Fig.40.

By activating the thermal flag of the model, the self-heating effect is considered. The expected outcomes are as follows: firstly, the load line is shifted downward, as the collector current diminishes with increasing dissipated power; secondly, since the device operates in Class A, it is anticipated that the device will dissipate more power when the input power is low. However, as the input power increases, the dissipated power will decrease, ultimately resulting in the cooling of the device once the maximum input power is reached; thirdly, the power gain has to drop too.

To obtain reliable results, the following parameters have been set in addition to those used earlier:

$$R_{th} = 536.25\ ℃/W$$

$$X_{TI} = -0.175$$

$$X_{T\beta} = -0.175$$

in particular R_{th} has been selected to allow a $\Delta T \approx 50\ ℃$, where $\Delta T = T_j - T_a$.

The results are presented:

- **Verification of the quiescent point.**
  In Fig.37, it is illustrated the expected results, indeed, it can be observed the variation of the slope in the I_C curve as the DC power increases, also the shift of the load line is shown, confirming the expected outcome for this result.

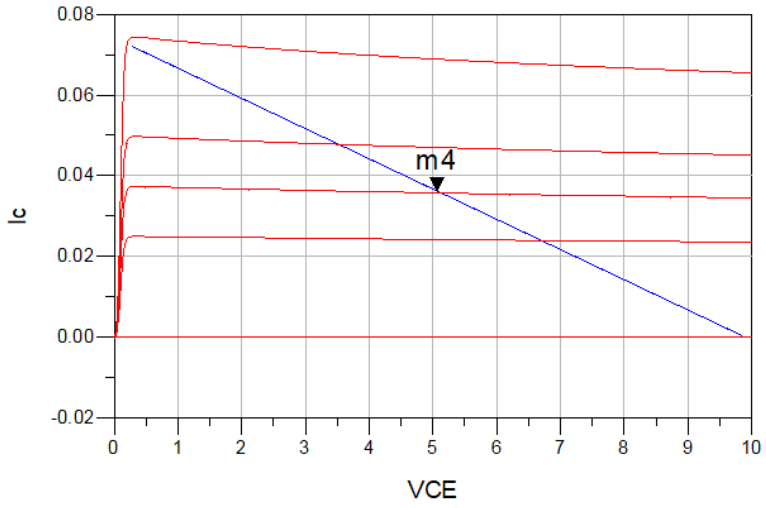

Fig.37 Quiescent point of the Class A when the thermal effect is included

- **Verification Pin-Pout characteristics and Gain**.
  In Fig.38 the Pin-Pout characteristic is shown with a decrease in the saturation point of 0.24 dBm with respect the case where no thermal effects are considered, whereas, in Fig. 39 the gain versus the input power is shown; the gain suffers of a loss of $1.135\ dB$ with respect to the previous case. This also confirms the expected outcomes.

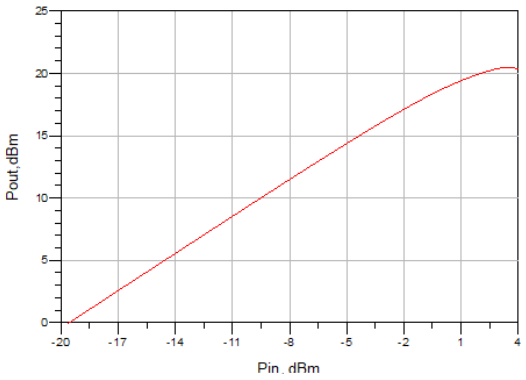

Fig.38 Pin-Pout characteristic for thermal effect is included

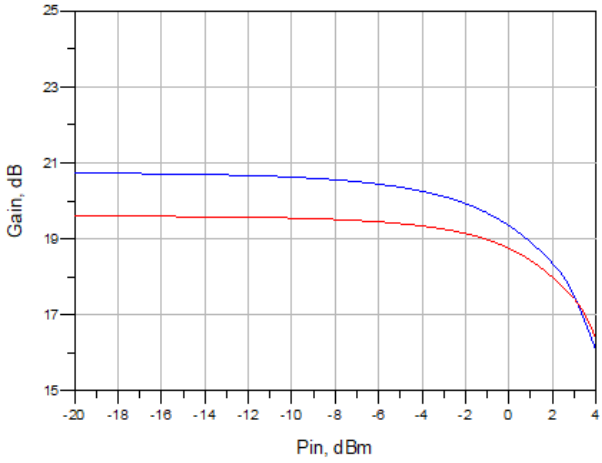

Fig. 39 Comparison of Gain versus Pin when the thermal effect is included (blue curve) and when it is not accounted for (red curve)

- **Verification of the dissipated power and junction temperature.**

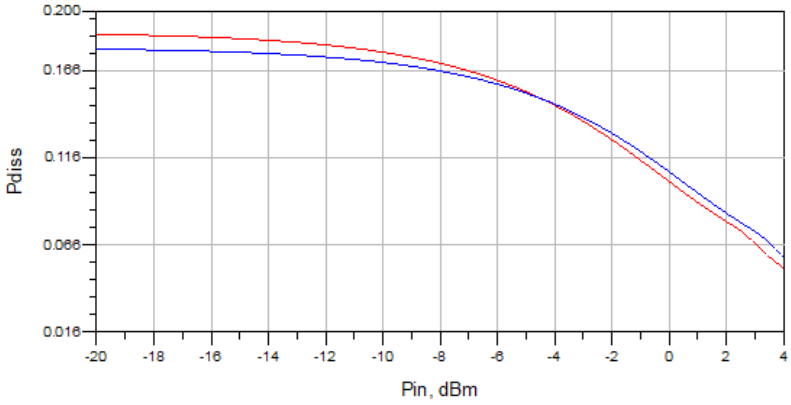

Fig.40 Dissipated power $Watt$ versus the Input Power in dBm. The red curve is illustrating the dissipated power when no thermal effect is taken into account, whereas the blue curve is illustrating the dissipated power when the thermal effect is accounted for.

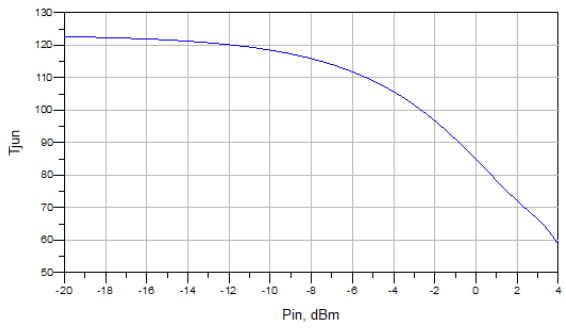

Fig.41 Junction Temperature in Celsius versus the Input Power in dBm

In Fig.40 the dissipated power is decreasing as the input power increases, and an analogous behavior is illustrated for the junction temperature, confirming the anticipated outcomes.

Lastly, the effects of the collector-emitter parasitic capacitance and its compensation are shown.

Indeed, up to now, no collector-emitter capacitance has been considered; once the capacitance is introduced, for this instance it is set at $C_{CE} = 750\ fF$, the load line assumes the form illustrated in Fig.42 as it introduce a phase difference between the V_{CE} and I_C.

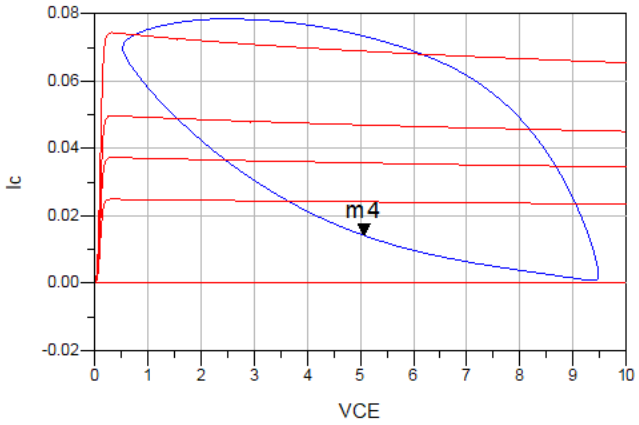

Fig.42 load line behavior when a collector-capacitance is introduced

The quiescent point is moved downward, leading to a reduced biasing collector current and to a reduced voltage swing, with detrimental effects on the gain and increasing the total distortion.

To mitigate this effect a matching network is used to compensate for the phase variation. In Fig.43 is shown the schematic with the added matching network.

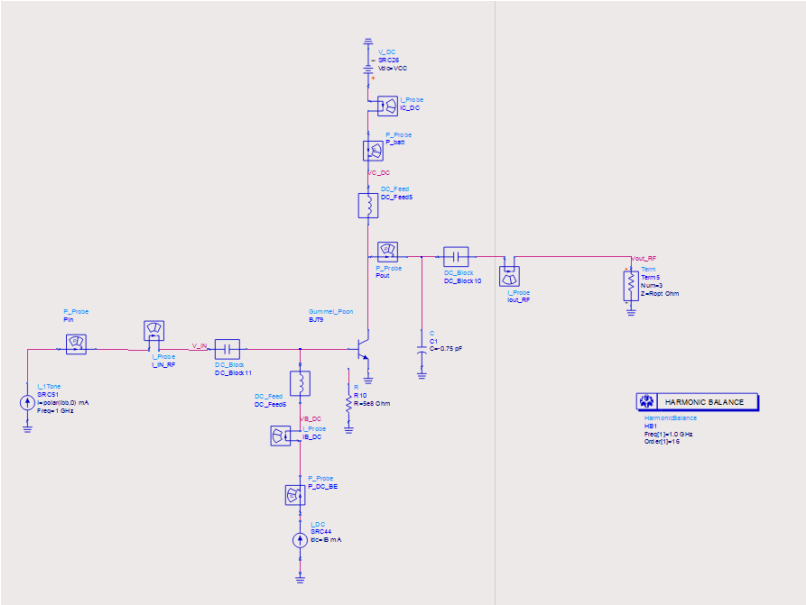

Fig.43 Class A schematic with the compensating capacitance

The simulation of the schematic in Fig.43 leads to the plot of the load line, already illustrated, in Fig.37.

4.1.2. Class B amplifier and testing

The class B amplifier with tuned load is considered. In the biasing condition the base current is changed [3], whereas $V_{CE,max} = 10\ V$ and $I_{C,max} = 75\ mA$ are left identical to the class A leading to the same optimum load:

$$R_{opt,B} = \frac{V_{CE,max}}{I_{C,max}} = \frac{10\ V}{75\ mA} = 133\ \Omega.$$

The biasing current I_B is set to 5% of the maximum base current supported by the device, i.e.

$$I_{B,Q} = \frac{5}{100} \cdot \frac{I_{C,max}}{\beta_F} = 37.5\mu A$$

However, the polarization of the base-emitter junction must occur in voltage, as a current generator would fix the current in DC, preventing its variation and causing the input voltage to reach unrealistic values of the order $10^4\ V$. Therefore, the V_{BE} is chosen so to guarantee the value of $I_{B,Q}$ resulting in

$$V_{BE,Q} = 0.709\ V$$

The schematic for the simulation is shown in Fig.44.

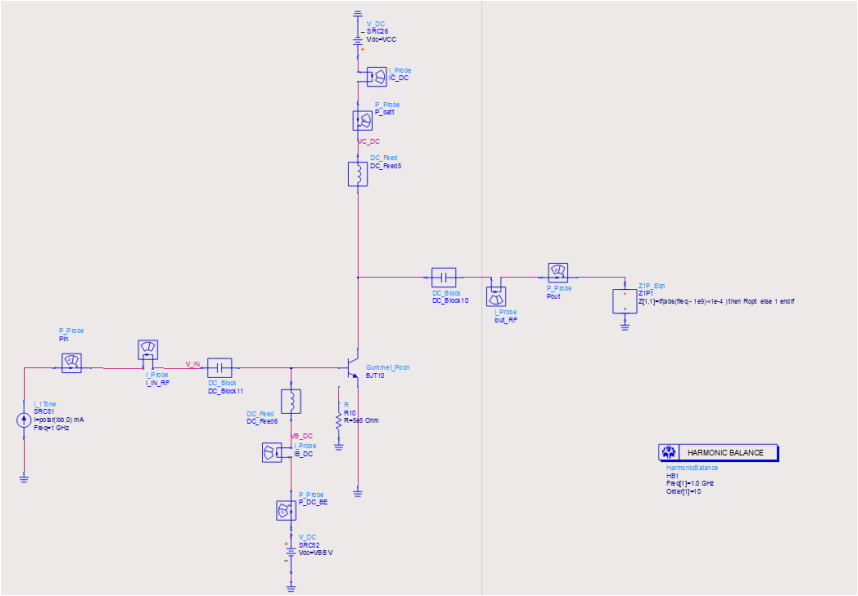

Fig.44 Tuned Class B amplifier schematic.

The Z1P component has been introduced to implement the ideal tuned load, as it allows for modeling impedances using mathematical equations that describe its behavior.

Therefore, the equation used in the simulation is

$$Z_{load}(f) = \begin{cases} R_{opt} & \text{if } |f - f_0| < 10^{-4} \\ 0.1 & \text{otherwise} \end{cases} \tag{4.31}$$

where f_0 is the fundamental, i.e. $f_0 = 1\ GHz$.

The auto-polarization effect of the BJT complicates the proper design of Class B. Specifically, I_B and I_C are interdependent, which contrasts with the behavior of a FET [3], where the controlling voltage gate-source v_{GS} can be adjusted around the threshold, without being affect by the biasing drain current I_D, to achieve the correct bias point. Consequently, most of the results presented are a rough approximation. Nevertheless, the main outcomes illustrating the thermal effects are accurately captured by the simulation.

As was done for Class A, the behavior of the tuned Class B is also discussed, both with and without the presence of thermal effects. In either case the two junction capacitances have been set so to have a reasonable value of the gain but also to have a load-line more similar to that of a class B, i.e.

$$C_{JC0} = 10\ fF$$
$$C_{JE0} = 800\ fF$$

First, the outcomes for the tuned class B without the thermal effect are shown.

- **Quiescent point and load-line**
  As did in the case of class A, the quiescent point and load-line are present in Fig.45

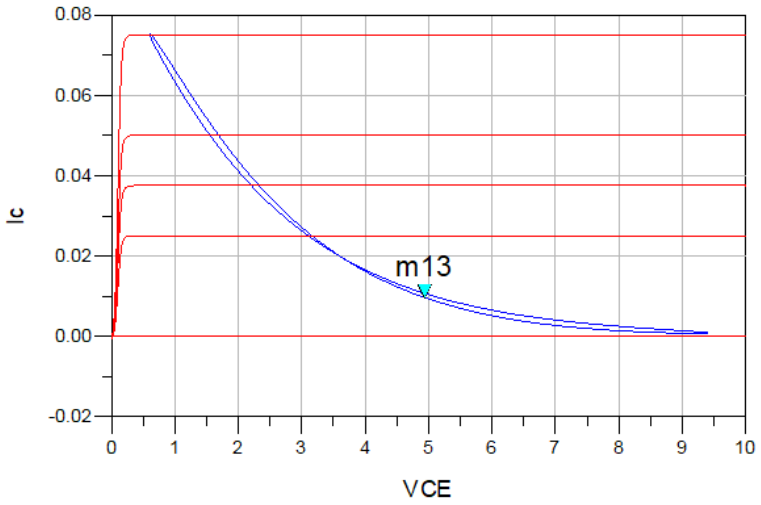

Fig.45 Quiescent Point and load line of the tuned Class B where m_{13} is the bias point, when the thermal modelling is deactivated

- **Pin-Pout characteristic and Gain**

  In Fig.46 and Fig.47 the Pin-Pout characteristic and the gain against the input power are illustrated. From which is possible to notice the expansive nature [3] of the device, i.e., rather than moving toward saturation both the gain and the outpower keep increasing as the input power increases.

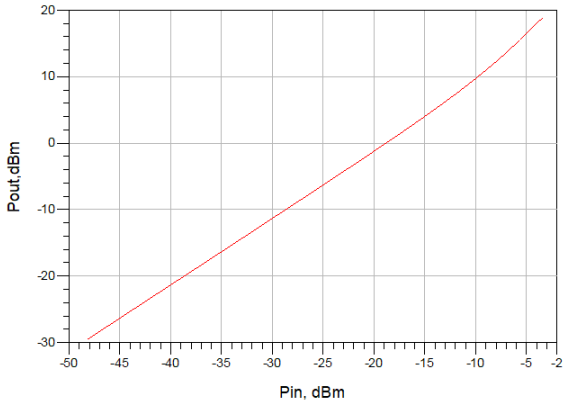

Fig.46 Pin – Pout characteristic in logarithmic scale when the thermal modelling is deactivated

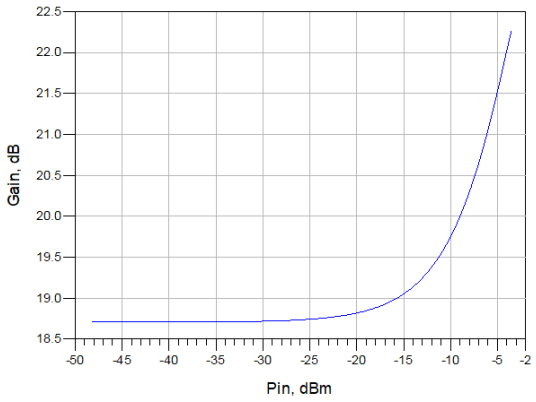

Fig.47 Gain versus Pin in logarithmic scale when the thermal modeling is deactivated

- **Dissipated power and Junction Temperature.**
  As seen for the Class A when the thermal model is deactivated, the junction temperature is as the same as the room temperature. The simulation results regarding the dissipated power as a function of the input power will be shown in Fig.51.

After presenting the Class B results without thermal effects, the amplifier results are now illustrated with thermal effects considered.

- **Quiescent point and load-line curve**

  From the comparison between Fig.48 and Fig.45, it is seen that the quiescent point is shifted downward making the amplifier behavior more similar to the class B behavior. However, the maximum voltage swing and the maximum collector current are decreased too.

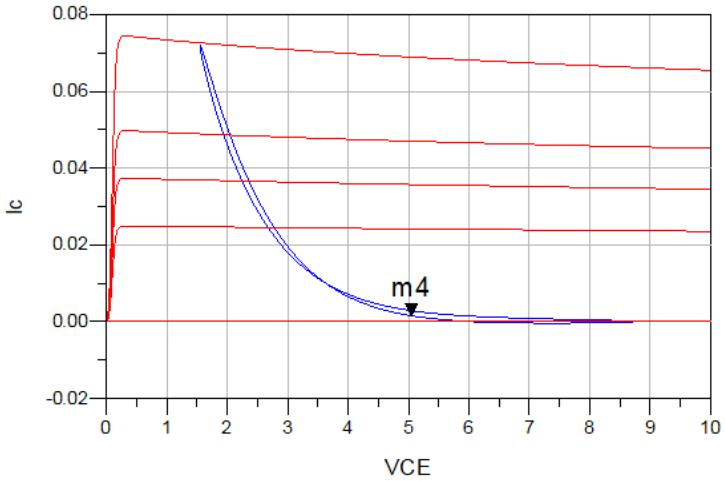

Fig.48 Quiescent point and load-line curve with thermal effect included

- **Pin-Pout characteristic and Gain curve.**

From the comparison of Fig.49 and Fig.46, it is noticed that the outpower is decreased for the same input power; indeed this is proved by the fact that, as shown in Fig.50,the gain is also decreased with respect to the gain when the thermal effect was not accounted for. Moreover, the expansive nature of the device is further accentuated.

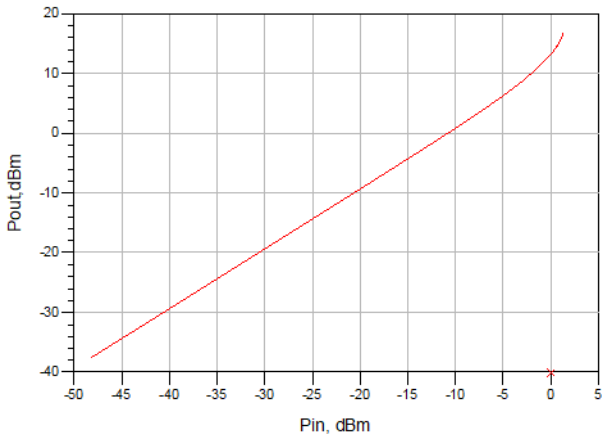

Fig.49 Pin-Pout characteristic with thermal effect included

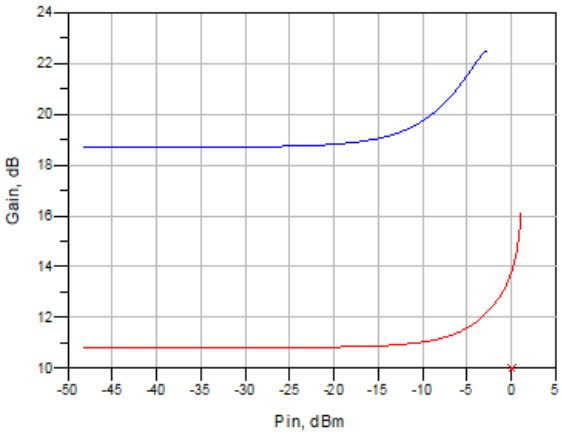

Fig.50 Gain in dB versus Input Power in dBm
with thermal effect included (red curve) and when the thermal effect is not included (blue curve)

- **Dissipated power and junction temperature.**

Fig.51 and Fig.52 are illustrating the behavior of the dissipated power and of the junction temperature as the input power increases. These plots confirm the correct behavior of the class B, as the dissipated power from the device has to increase as the input increases, leading to the increasing of the junction temperature.

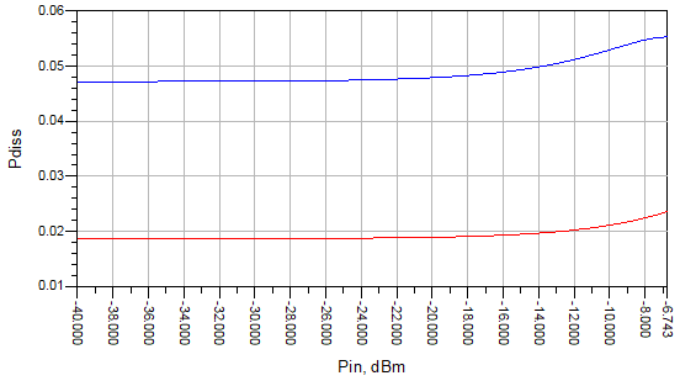

Fig.51 Plot of the dissipated power versus the input power. The blue curve shows the dissipated power when the thermal effect is not account for, whereas the red curve is showing the dissipated power when such effect is accounted for.

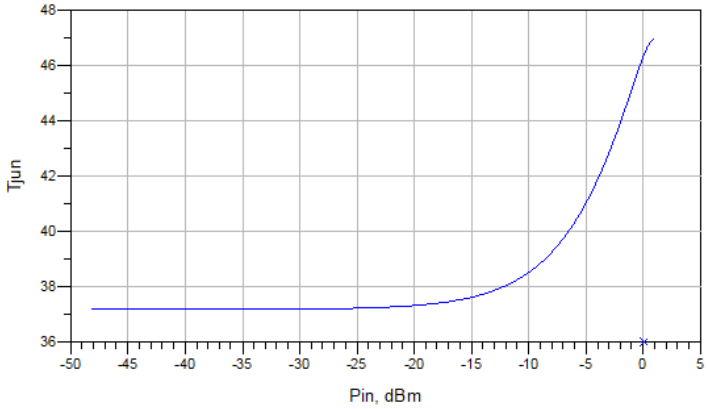

Fig.52 Plot of the junction temperature versus the input power

Finally, the effect of the collector- emitter capacitance C_{CE} on the load-line, when the thermal effects are included, is shown. As done previously for the class A in 4.1.1 the collector-emitter capacitance is set to

$$C_{CE} = 750\ fF$$

leading to a form of the load-line shown in Fig.53.

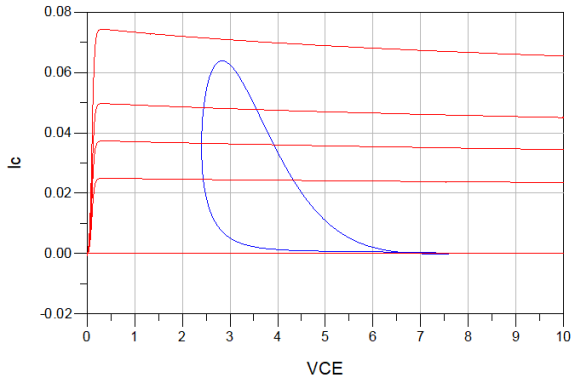

Fig.53 Load-line of the class B affected by the presence of C_{CE}

As observed in 4.1.1, the presence of the collector-emitter capacitance leads to a severe drop in the gain of the device possibly leading to instability. Also in this case, it is possible to compensate this effect using a matching network.

5.Conclusions

Based on the previous discussion, it can be concluded that this model is useful for applications in microwave electronics, providing an alternative version of the electrothermal self-consistent Gummel-Poon model, suitable for Si BJTs and GaAs HBTs.

As extensively described, following the transition from the Ebers-Moll model to the Gummel-Poon model, the key equations were implemented in the Keysight ADS software, exploiting the SDD element, to account for on how transistor parameters depend on temperature.

In particular, the following simulations were conducted:

- DC simulation to verify the correct dc operation of the implemented model;
- Small-signal simulation and S-parameters for frequency operation verification;
- Harmonic Balance simulation for verification during the transient phase of the fundamental parameters describing Class A and Class B amplifiers.

These simulations as expected, particularly for GaAs HBTs, show that the I_C vs V_{CE} output characteristic curves exhibit a negative slope.

In light of this, it was shown that the self-heating effect has a significant impact on Class A and Class B amplifier's performance, as it causes a variation in the shape or slope of the load curve, leading to substantial loss of gain and stability.

Fig.40, Fig.41, Fig.51, Fig.52 illustrate how, in the case of Class A, the dissipated power and, consequently, the junction temperature decrease as the input power increases, whereas for Class B, there is an increase in dissipated power and a subsequent rise in junction temperature with increasing input power.

In conclusion, the implemented model can be used as a starting point for the development of more sophisticated analysis methods in high-frequency and high-power electronics, due to the interoperability between the electrical and thermal models.

Bibliography

[1] G. Massorbio and P. Antognetti, Semiconductor Device Modelling With Spice, McGraw-Hill,Inc., 1993.

[2] F. Bonani, S. D. Guerrieri, G. Masera and G. Piccinini, Dispostitivi e tecnologie elettroniche, CLUT, 2007.

[3] G. Ghione and M. Pirola, Microwave Electronics, Cambridge University Press, 2018.

[4] M. E. Klausmeier-Brown, P. D. DeMoulin, M. S. Lundstrom, M. R. Melloch and S. P. Tobin, "Measurement of bandgap narrowing effects in p-GaAs and implications for AlGaAs/GaAs HBT performance," *IEEE Transactions on Electron Devices,* vol. 35, no. 12, pp. 2445-, 1988.

[5] C. Persson, U. Lindefelt and B. Sernelius, "Bandgap Narrowing in n-type and p-type 3C-, 2H-, 4H-, 6H-SiC, and Si," *J.Appl.Phys.,* vol. 86, no. 8, pp. 4419-4427, 1999.

[6] H. Lanyon and R. Tuft, "Bandgap narrowing in moderately to heavily doped silicom," *IEEE Transactions on Electorn Devices,* vol. 26, no. 7, pp. 1014-1018, 1979.

[7] S. Sze and K. K. Ng, Physics of semiconductor devices, Wiley Online Library, 2007.

[8] J. Erber and J. Moll, "Large-signal behavior of junction transistor," *Proceedings of the IRE,* vol. 42, no. 12, pp. 1761-1772, 1954.

[9] I. Getreu, Modeling the Bipolar Transistor, Beaverton, Oregon: Tektronix Inc., 1976.

[10] B. Chawla and H. Gummel, "Transition region capacitance of diffused p-n junctions," *IEEE Transactions on Electron Device,* vol. 18, no. 3, pp. 178-195, 1971.

[11] H. Gummel and H. Poon, "An integral Charge Control Model of Bipolar Transistor," *Bell. Syst. Tech. J.,* 1970.

[12] M. Panish and H. Casey, "Temperature Dependence of the Energy Gap in GaAs and GaP," *Journal of Applied Physics,* vol. 1, no. 40, pp. 163-167, 1969.

[13] Keysight, "Advanced Design System Product Documentation," [Online]. Available: https://docs.keysight.com/display/support/ADS+Product+Documentation. [Accessed March 2025].

[14] Jianjun and Gao, Heterojunction Bipolar Transistors For Circuit Design, Microwave modelling and parameter extraction, Wiley Higher Eduction Press, 2015.

[15] J. Mcmacken, J. Gering and D. Halchin, "HBT Modelling," *IEEE Microwave Magazine,* vol. 9, no. 2, pp. 48-71, 2008.